Case Studies in Construction Materials 21 (2024) e03944

Contents lists available at ScienceDirect

Case Studies in Construction Materials

journal homepage: www.elsevier.com/locate/cscm

Microstructural properties of Asian hornet nest paper-like materials: Preliminary step towards biomimicry materials for civil engineering applications

Naim Sedira [a,b,*], Jorge Pinto [a,b], Ana P. Gomes [c,e], Miguel C.S. Nepomuceno [b,c,d], Sandra Pereira [a,b]

[a] University of Trás-os-Montes e Alto Douro (UTAD), Vila Real, Portugal
[b] CMADE - Centre of Materials and Building Technologies, UBI, Covilhã, Portugal
[c] University of Beira Interior (UBI), Covilhã, Portugal
[d] Lab2PT, Landscape, Heritage and Territory Laboratory, Guimarães, Portugal
[e] AEROG-LAETA, Aerospace Sciences department, UBI, Covilhã, Portugal

ARTICLE INFO

Keywords:
Biomimicry
Microstructure
Vespa velutina nigrithorax
Nest
XRD
Leaves structure

ABSTRACT

This paper presents a comprehensive examination of the microstructure and mineralogy of the paper-like material found in Asian hornet nests (referred to as AHN P-LM) and the nearby tree leaves, utilising scanning electron microscopy with energy dispersive spectroscopy (SEM-EDS) and X-ray diffraction (XRD). The analysis conducted through SEM-EDS demonstrates that AHN P-LM is primarily composed of plant fragments, with slight traces of inorganic substances (such as CaOx). The thread-like morphologies observed in the SEM analysis, which are linked to the secretion of hornets, warrant attention due to their significance in understanding the microstructure of AHN P-LM. The presence of nitrogen (N) in the EDS analysis of AHN P-LM, in contrast to its absence in analysed leaves, strongly implies that the nitrogen originates from hornet saliva. Additionally, SEM-EDS analysis revealed the impact of chemical composition variations on colour differences within AHN P-LM. Furthermore, X-ray diffraction analysis on ash samples from AHN P-LM confirmed the presence of minerals such as quartz, lime, phlogopite, and microcline. These findings about mineral composition align closely with results obtained from SEM-EDS analyses, presenting various aspects related to understanding the structure and compositional makeup of AHN P-LM. Biomimicry principles can be applied to draw inspiration from the AHN P-LM for replication in the civil engineering field, facilitating innovative solutions. Understanding hornet behaviour and nest material composition is essential. Future outlook includes utilising these materials in wood construction, 3D printing for structural components, shelters, infrastructure repair, green building, and architectural innovation.

1. Introduction

The genus Vespa contains 22 species of hornets, which are highly social wasps. One or more queens and their offspring construct large nests maintained by these conspicuous insects [1]. These large nests may contain a few hundred to several thousand hornets [2].

* Corresponding author at: University of Trás-os-Montes e Alto Douro (UTAD), Vila Real, Portugal.
E-mail address: naimsedira@utad.pt (N. Sedira).

https://doi.org/10.1016/j.cscm.2024.e03944
Received 31 May 2024; Received in revised form 8 October 2024; Accepted 1 November 2024
Available online 6 November 2024

Vespa velutina Lepeletier, 1836 (Hymenoptera: Vespidae) is an Asian hornet native to the mountains of Southeast Asia from Kashmir to Malaysia, spreading eastwards to Taiwan, south-eastwards to Sulawesi, the Sunda islands, and Timor. There are 14 subspecies of this taxon [3,4], which differ from each other morphologically primarily in their body colours. Among these are Vespa velutina nigrithorax du Buysson, 1905 (South China) subspecies [5]. The nests of Vespa velutina nigrithorax (du Buysson) have become a topic of interest due to the invasive nature of this species. Vespa velutina nigrithorax, commonly known as the yellow-legged Asian hornet, has rapidly spread across Europe, posing a significant threat to European pollinators [6]. The Yellow-legged hornet, Vespa velutina, is an invasive species from Asia. It was first recorded for the first time in Europe (France, Lot-et-Garonne) by Haxaire et al. in 2005 [7]. The hornets were introduced via trade through southwestern France in or before 2004 [8] and have since spread across several countries, including northern Spain, Portugal, Italy, Germany, Mallorca Island, the Channel Islands [9], and the UK [10]. Vespine wasps, similar to polistine wasps, engage in nest construction by biting off plant fibres or other fibrous materials. These materials are subsequently blended with saliva, transforming them into a pulpy consistency. The resulting pulpy substance is then stretched and shaped into a building material. This process shares similarities with the techniques employed in commercial paper manufacturing. Conversely, it is important to note that the specific materials used for nesting vary depending on each species. Plant fibre is often considered the optimal material due to its proximity, ability to facilitate the construction of a lightweight yet durable nest, requirement of a minimal amount of material, and ease of nest modification [11]. The nests of Vespa velutina nigrithorax are composed of organic materials such as wood from forest species, leaves, and grasses. The nests are formed by the agglomeration of tiny particles spatially organised in brown and beige strips. The nests' main chemical constituent is cellulose, composed mainly of carbon and oxygen, with small amounts of other microelements. The nests are ovoid-shaped and range from 18.7 cm to 45.0 cm in diameter and 19.2 cm to 65.0 cm in length. The nests are built in the spring as primary nests, then secondary nests are built during summer. The secondary nests are larger and more exposed in places such as tree canopies. The nests of Vespa velutina nigrithorax are important to study to understand the behaviour and adaptability of this invasive species [12,13]. The nests of Vespa velutina nigrithorax (du Buysson) comprise a large comb nest contained within a protective outer envelope. To shield their nest combs and ensure their safety, the wasps construct an outer envelope structure that safeguards the nest from inclement weather conditions (such as extreme heat and cold) and prevents predators from gaining access to the nest. Furthermore, the envelope structure is constructed using multiple layers of plant material and saliva, rendering it water-resistant and protecting the nest from harm [14]. The outer envelope nests of Vespa velutina are constructed using paper-like fibres. These fibres are made from wood pulp obtained from various sources. The hornets chew the wood pulp and mix it with their oral secretions to form the outer envelope nests [15]. This process allows them to create intricate and durable structures that protect and support their combs and colonies.

In 1997, Janine M. Benyus introduced the term "Biomimicry", derived from the Greek words "bios", meaning "life", and "mimesis", meaning "imitation" [16,17]. Biomimicry involves studying and imitating nature's strategies, often used by designers to address human challenges and help solve problems [18]. According to the Biomimicry Institute [19], biomimicry is a practice that draws inspiration from nature to find innovative solutions to human design challenges, fostering hope. In civil engineering, biomimicry has emerged as a novel approach to tackle sustainability challenges and complex managerial issues within the construction sector. Research has delved into its application in architecture, building construction, and civil engineering, aiming to develop a clear understanding of its implementation [20]. Examples include emulating load-carrying mechanisms found in trees to design resilient bridges [21], mimicking the self-healing properties of cement paste inspired by bone structure [22], and adopting biomimetic materials and designs for resilient civil infrastructure systems. Such research endeavours aim to bridge the gap between biomimetic technologies and commercial building development, thereby enhancing structural stability, energy efficiency, and sustainability in the built environment [23–25]. Daniel G. Soltan and Victor C. Li [26] investigate the practical application of nacre's composite design on a scale relevant to infrastructure. They leverage the "distributed microcracking" behaviour of strain-hardening cementitious composites (SHCCs) and mimic nacre's deformation mechanisms, mainly through an alternating layering approach. Significant performance improvements are achieved. This approach, employing a geotextile mesh and high-strength SHCC, outperforms monolithic SHCC in tension, compression, and flexure, demonstrating promising prospects for infrastructure applications. Building upon this biomimicry strategy, P. Gunasekaran et al. [27] extend the concept to construction, particularly in thin shell structures inspired by the shape of the human skull. Ansys 18.1 software is used for a mesh convergence study, optimising parameters like thickness and span based on scanned skull models. The study predicts the most efficient model by comparing equivalent stress with theoretical values. This approach highlights the symbiotic relationship between the environment and construction, indicating the integration of natural forms for sustainable solutions. Additionally, M. Vishali et al. [28] examine the behaviour of reinforced concrete trapezoidal frames under lateral loading and various interface materials, establishing an effective diagonal width to streamline the design process. The investigation focuses on trapezoidal infilled frames, which have received less attention than rectangular and square frames. The research enhances understanding of the interaction and behaviour of trapezoidal infilled frames in industrial buildings. To facilitate design, an effective diagonal width was devised for different interface materials based on the relative stiffness of various frame cross-sections, further validated using an ideology framework from biomimicry and a one-sixth scale model. Another study explores termite-inspired construction materials aimed at environmental mitigation [29]. Termite mounds, naturally formed structures, comprise a blend of soil particles and termite saliva, containing polysaccharides and enzymes that aid soil stabilisation and adhesive properties. By emulating this natural process, researchers have manufactured clay bricks using a combination of clay soil and cassava flour to introduce polysaccharides. These clay bricks, integrating cassava flour to enhance polysaccharide content, demonstrate superior strength when containing 1.5 % cassava flour (4.28 MPa), surpassing the strength of traditional burnt clay bricks.

In a previous study, N. Sedira et al. [14] examined the internal architecture, materials, and functionality of Asian hornet nests, revealing their intricate design. Understanding this architecture, including the outer envelope and combs, provides an understanding of materials, design, and engineering principles applicable to civil engineering. The study also explored construction principles

relevant to civil engineering. Through the application of biomimicry, Asian hornet nests offer valuable perspectives on designing stable structures. Therefore, this study aimed to thoroughly analyse the nest paper-like material microstructure and mineralogy. To accomplish this objective, initial SEM-EDS and XRD analyses were conducted on the tree leaves near the location of the case study nest. Following this, SEM-EDS analyses were performed on the nest's paper-like materials, and both SEM-EDS and XRD analyses were carried out on the ash derived from these materials. These analyses also aimed to identify and characterise any inorganic substances present within the composition of the nest paper-like material.

2. Concept

Drawing inspiration from natural structures, such as insects' and birds' nests, to inform advancements in civil engineering is known as "biomimicry" or "bioinspiration". Biomimicry involves studying natural systems, processes, and organisms to gain understanding and inspiration for solving human design challenges [30]. In the case of using wasp and hornet nests as inspiration in civil engineering, we can examine the structural integrity, material properties, and construction techniques employed by these insects to build their nests. This knowledge can then be applied to design more efficient and sustainable structures in civil engineering, such as buildings, bridges, or infrastructure. By mimicking the strategies and techniques found in the nests, we can develop innovative solutions that are more sustainable and often more resilient and adaptive to changing environmental conditions.

3. The case study of the Asian hornet nest

The Asian hornet nest (AHN) of the case study is an oval structure several centimetres in diameter. It can be identified by its distinctive yellowish-brown colour and papery texture. AHNs are commonly found in trees and shrubs but are additionally observable in buildings or other man-made structures. Wasp and hornet nests tend to be more prevalent in warmer and humid climates.

3.1. Nest collection

An AHN of Vespa velutina nigrithorax (du Buysson) was found in a Populus tree in Amarante in the Tâmega e Sousa subregion of northern Portugal. A main branch of the tree was cut to remove the nest from its original location. Larvae, pupae, dead, and remaining eggs were removed from the nest. A laboratory has been maintaining precise temperature and humidity levels since December 2021, and the nest has been preserved.(Fig. 1)

3.2. Samples collecting for SEM-EDS analysis

Small fragments were cut from the outer envelope and cell walls of the AHN (Fig. 2) and were then observed using an SEM (HITACHI S-3400N). The SEM-EDS analysis reveals the structure, surface morphology, and chemical composition of the two Asian hornet nest paper-like material fragments. Moreover, Fig. 3 presents the Castanea sativa Mill – The European Chestnut, European nettle tree (Celtis australis), and Hazel (Corylus avellana. L) leaves.

3.3. SEM-EDS of the AHN P-LM

This study took a sample from each tree leaf surrounding the AHN. The samples were then analysed using SEM-EDS with the HITACHI S-3400N scanning electron microscope to examine their structure and composition. Further, small material portions were removed from both the outer envelope and cell walls of the P-LM in the AHN. The SEM-EDS analysis shows important information about the detailed structure, surface morphology, and precise chemical composition of these fragments of the AHN P-LM.

(a) (b)

Fig. 1. (a)- Combs, and (b)- Outer envelope in large Asian hornet nest.

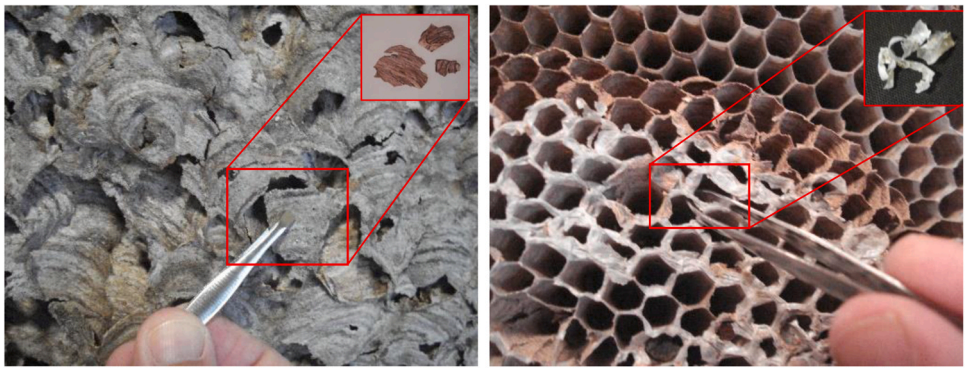

(a) (b)

Fig. 2. Sample collection from: a) the outer envelope; b) the cell walls comb of the AHN.

(a) European nettle tree (Celtis australis)

(b) Castanea sativa Mill – The European Chestnut

(c) Hazel (Corylus avellana. L)

Fig. 3. Tree leaves near the AHN a) Castanea sativa Mill – The European Chestnut; b) European nettle tree (Celtis australis); c) Hazel (Corylus avellana. L) tree.

SEM-EDS analyses were performed to compare the paper-like materials found in the nests of Asian hornets and the ashes of tree leaves. This comparison aims to contribute to a deeper understanding of the source of the AHN P-LM. The mineral composition of the ashes from tree leaves was identified through SEM-EDS analysis and then compared to the mineral composition of the ash derived from the paper-like material of Asian hornet nests. Furthermore, SEM-EDS analysis was used to investigate the distinct colours of the outer envelope of the AHN P-LM to discern any variations in composition and microstructure among the different coloured in the outer envelope P-LM.

3.4. X-ray diffraction (XRD)

X-ray diffraction (XRD) data were systematically collected at room temperature utilising a Rigaku model D-Max III/C X-ray diffractometer equipped with a Cu tube and K-α radiation (40 kV, 40 mA). The diffraction patterns were recorded over a comprehensive 2θ operational range from 5° to 90° [31]. This experimental setup facilitated the identification of potential mineral phases present in the different analysed ashes.

4. Results and discussion

4.1. SEM-EDS analysis of the tree leaves

This section comprises two primary subsections. The initial subsection focuses on the SEM-EDS analyses conducted on the raw tree leaves, followed by subsections dedicated to examining the ashes derived from these leaves. The second primary subsection focuses on the SEM-EDS analyses conducted on various components of the paper-like material discovered in the nest of the Asian hornet (AHN P-LM), with subsequent subsections exploring the characterisation of the ashes derived from the aforementioned AHN P-LM.

4.1.1. SEM-EDS analysis of the tree leaves materials (raw leaves)

The leaves of three tree species Corylus avellana (Hazel), Chestnut, and European nettle tree were subjected to SEM-EDS analysis in the proximity of the collected Asian hornet nest (The case study nest), and the results are outlined in Table 1, and (Before incineration).

4.1.1.1. SEM analysis of the tree leaves materials

4.1.1.1.1. European nettle tree (Celtis australis) leaf. Fig. 4 presents the microstructure of the European nettle tree (Celtis australis) leaf, illustrating various compositions. Fig. 4 provides the surface of the (Celtis australis) leaf, providing a close-up view. The outermost layer of the leaf, known as the epidermis, is visible on both sides, referred to as the upper and lower epidermis, respectively. Botanists term the upper side the adaxial surface (or adaxis) and the lower side the abaxial surface (or abaxis). The epidermis helps regulate gas exchange [32,33]. The main feature mentioned here is the cuticle, which forms a protective layer covering the leaf surface. Additionally, multibranched trichomes are visible on the leaf surface. These multi-branched trichomes on the abaxial surface (mbt) are hair-like structures found on the underside of the leaf, possibly serving protective or sensory functions [34], as shown in Fig. 4a. The abaxial surface of the (Celtis australis) leaf also exhibits a distinctive appearance resembling lips surrounding the openings called "stomata (St)", specialised pores on the leaf surface that regulate gas exchange and transpiration. Each Stomata is encircled by two guard cells, which regulate its opening and closing [35–39]. Together with specialised stomata resembling lips, these trichomes are essential in regulating gas exchange and transpiration, significantly contributing to the leaf's overall functionality and environmental adaptation. Fig. 4b presents a cross-section of the leaf's internal structure, providing a detailed examination of its composition, revealing the (Celtis australis) leaf as a dicot leaf. The protruding bumps observed on the lower surface of the leaf are leaf cuticles. The leaf cuticle is a barrier facilitating bidirectional substance transport between the plant and its surrounding environment; it protects against various stresses, including desiccation, UV radiation, and pathogen attacks [40,41]. Additionally, the cuticle is the primary barrier against uncontrolled water loss from leaves, fruits, and other essential parts of higher plants [42]. The layers of cells beneath the epidermis of dicot leaves are commonly referred to as the mesophyll. In the SEM image of the (Celtis australis) leaf presented in Fig. 4b, the mesophyll is positioned between the upper and lower epidermises [43]. Functioning as the internal ground tissue between the two layers of epidermal cells in the leaf, the mesophyll comprises two distinct types of tissues. Fig. 4c provides a closer look at the palisade parenchyma (also known as the palisade mesophyll), positioned beneath the upper epidermis [44]. Palisade cells (P), elongated and densely packed with chloroplasts, have an important role in photosynthesis. A small vascular bundle (svb) is embedded within these cells and responsible for fluid transport throughout the leaf. Furthermore, Fig. 4d zooms in on the parenchyma (denoted as "s" in the SEM image) (or spongy mesophyll), a layer situated beneath the palisade mesophyll, characterised by loosely arranged, irregularly shaped cells, either spherical or ovoid, with fewer chloroplasts, facilitating gas exchange and containing noticeable intercellular air spaces (ac) [45,46]. Both layers of the mesophyll contain numerous chloroplasts. Notably, chloroplasts are exclusively found in guard cells among the epidermal cells.

Air cavities (ac) interspersed among the spongy parenchyma cells facilitate gas exchange within the leaf. The air space between the spongy parenchyma cells allows for gaseous exchange between the leaf and the external atmosphere through the stomata. In aquatic plants, the intercellular spaces in the spongy parenchyma aid in leaf flotation. The quantitative and spatial coordination of stomatal (st) pores in the epidermis and airspaces in the underlying mesophyll tissue are essential for efficient gas exchange in the leaf [47,48]. Stomata regulate gas exchange between the interior of the leaf and the external environment, facilitating the uptake of carbon dioxide

Table 1
Chemical composition of the different tree leaves around the hornet nest (Before calcination).

Element	Weight percentage (wt%)		
	Hazel (Corylus avellana. L)	Castanea sativa Mill – The European Chestnut	European nettle tree (Celtis australis)
Carbon	58.79	61.44	56.80
Oxygen	38.05	36.63	39.96
Magnesium	0.41	-	0.14
Aluminium	0.15	-	-
Silicon	0.25	-	0.79
Phosphorus	0.22	0.20	0.14
Potassium	1.02	1.24	0.61
Calcium	0.80	0.17	1.45
Iron	0.16	-	-
Copper	0.17	0.19	-
Sulphur	-	0.13	0.11

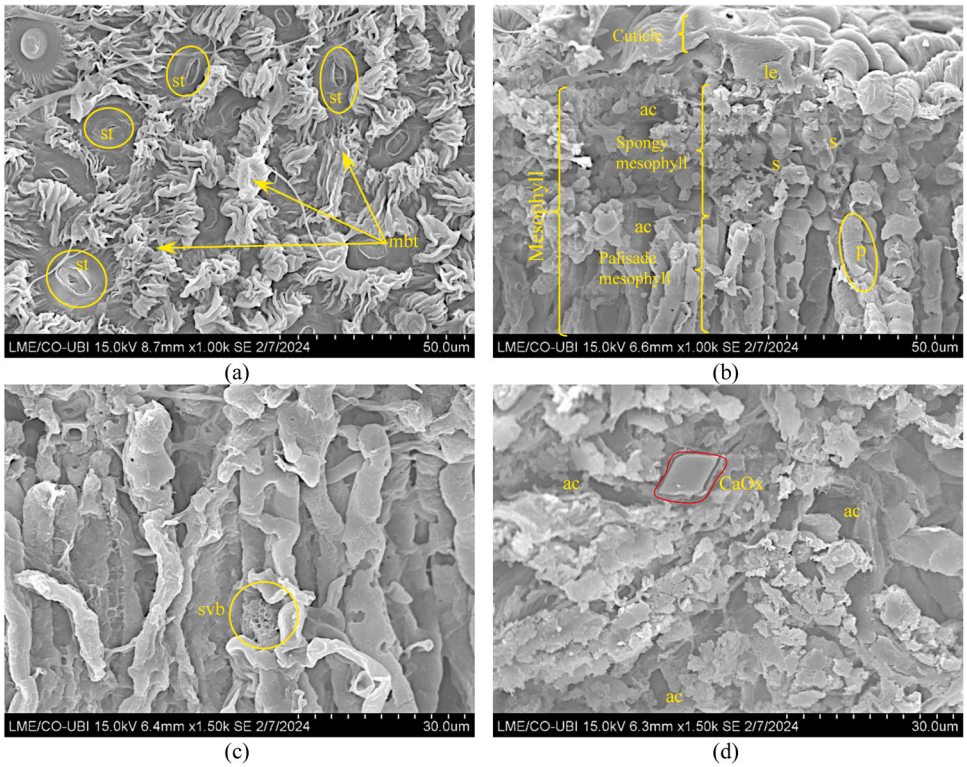

Fig. 4. SEM image of European nettle tree (Celtis australis) leaf in different positions: (a): the surface of (Celtis australis) leaf; (b): Overall cross-section position of the leaf microstructure; (c): cross-section position present palisade parenchyma cells with small vascular bundle in the middle; (d): cross-section position present spongy mesophyll. Abbreviations: Cuticle on top of the leaf microstructure; (le): Lower epidermis; (st): stomatal from European nettle tree (Celtis australis) leaf have the appearance of lips that surround the opening; (svb): small vascular bundle; (mbt): multibranched trichomes on the abaxial surface; (P): palisade cell; (ac): Air cavity; (s): Cells of the spongy parenchyma; (ch): Chloroplasts; (CaOx): calcium oxalate crystals.

(CO_2) required for photosynthesis and the release of oxygen (O_2) produced during photosynthesis, as well as the loss of water vapour (transpiration).

SEM analysis of (Celtis australis) leaf revealed the presence of calcium oxalate (CaOx) crystals in the spongy mesophyll cells, as shown in Fig. 4d. The crystals were found to be formed in crystal idioblasts with specific geometric shapes [49]. The crystals' ultrastructure was observed to be formed from parenchyma cells associated with mesophyll. CaOx crystals are present in all plant organs; in leaves, crystals idioblasts are mainly located within mesophyll and bundle sheath extension [50,51].

4.1.1.1.2. Castanea sativa Mill – The European Chestnut leaf. SEM microanalysis of Castanea sativa Mill—The European Chestnut leaf (CSM-ECL), as shown in Fig. 5, reveals distinct morphologies and captivating complexity in the leaf's microstructure.

It is shown in Fig. 5,a that on the leaf's surface from a superficial external perspective, there are a series of multi-uniseriate hair-shaped structures. This series of multi-uniseriate hair-shaped structures corresponding to non-glandular trichomes uniseriate observed on the epidermal surface.

The non-glandular trichomes observed on the epidermal surface of CSM-ECL exhibit striking similarities to those documented in the SEM images of Rubus idaeus L. leaves, as detailed in the study by Mirosława Chwill & Mikołaj Kostryco1 [52]. These trichomes, discernible in the SEM image, appear as elongated structures protruding from the leaf's epidermis. The distinctive presence of non-glandular trichomes [42,43]. In the SEM image, these non-glandular trichomes appear as elongated structures emerging from the leaf surface, exhibiting a discernible morphology. Specifically, on the surface of the CSM-ECL leaf in the SEM image (Fig. 5), the non-glandular trichomes appear as slender and elongated hair-like structures, which indicates their widespread distribution across the leaf surface. Additionally, a few stomata were also observed on the surface of the Castanea sativa Mill (CSM-ECL) leaf (labelled as "st") in the SEM image (Fig. 5a). This observation shows that the stomatal complex of the leaf conforms to the Van Cotthem classification [53] as an anomocytic complex. Anomocytic stomata are characterised by the absence of surrounding subsidiary cells enclosing the guard cells, and they are directly embedded within the epidermal layer, illustrating a specific adaptation to environmental conditions. This finding indicates a strategic distribution of stomata aimed at optimising gas exchange and regulating transpiration rates effectively [54,55]. Furthermore, SEM images (Fig. 5c and d) illustrate the complex structure of the vascular bundle in the CSM-ECL. Vascular bundles are arranged parallelly along the length of the leaf, extending from the base to the tip. The vascular bundle in a dicotyledonous leaf comprises several distinct tissues: xylem, phloem, bundle sheath cells, parenchyma cells, and fibres, each component serving specialised functions [56,57]. The leaf's vascular bundle comprises the protoxylem and metaxylem, two distinct

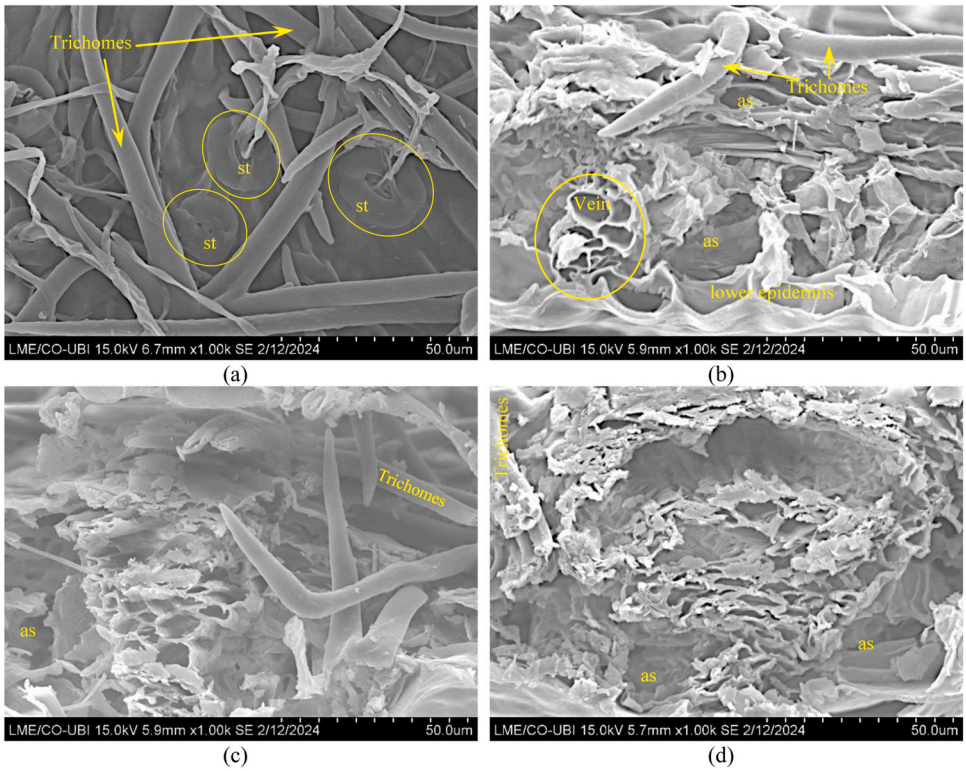

Fig. 5. SEM image of Castanea sativa Mill – The European Chestnut leaf in different positions. (a): Surface of the Castanea sativa Mill – The European Chestnut leaf; (b): Cross section position of the leaf; (c): SEM image shows xylem and phloem in the leaf vascular bundle from the leaf; (d): Big vascular bundles. Abbreviations: (as): air space; (st): stomata.

regions of xylem tissue serving vital roles in water and mineral transport. Protoxylem, positioned towards the centre of the vascular bundle, initiates differentiation first, featuring smaller cells with spiral or annular thickenings in their walls. Metaxylem, located closer to the leaf's periphery, follows protoxylem differentiation with larger, more mature cells possessing secondary cell wall thickenings, notably lignin deposits. Together, these regions facilitate efficient water and mineral uptake from the roots, distributing them throughout the leaf and the rest of the plant. Their integration into the leaf's vascular system, alongside other tissues such as phloem, bundle sheath cells, and parenchyma cells, supports essential physiological processes, including photosynthesis, nutrient uptake, and overall growth, ensuring the plant's vitality and survival [58–60]. Additionally, phloem tissue primarily consists of sieve tube elements and companion cells. These components, known as phloem sieve elements (SEs) and companion cells (CCs), are integral to the plant's vascular system [61]. SEs are formed through asymmetric cell divisions of procambial cells adjacent to SEs and pericycle cells [62]. Phloem tissue facilitates the transport of organic nutrients, such as sugars produced during photosynthesis, from the leaves to other plant parts, including roots and developing fruits. Sieve tube elements form conduits through which phloem sap flows, while companion cells are important in metabolic support and nutrient transport regulation [63,64]. Surrounding the vascular tissues (xylem and phloem) are bundle sheath cells [65]. The circular arrangement of bundle sheath cells (Fig. 5d) protects the phloem and xylem networks from external forces, providing structural support and regulating material exchange between the vascular bundle and surrounding mesophyll cells.

4.1.1.1.3. Hazel (Corylus avellana. L) Leaf. Fig. 6 illustrates the SEM image of Corylus avellana L, a monoecious and wind-pollinated broadleaf species [66]. The SEM image in Fig. 6a illustrates the abaxial epidermal leaf surface of Hazel (Corylus avellana. L), displaying cuticular surfaces and multiple stomatal structures. The Hazel (Corylus avellana. L) leaf possesses trichomes (hair-like structures) on the lower epidermis that serve to deter herbivores and provide protection from harmful UV-B radiation by behaving as optical filters [67]. Furthermore, stomata (st) are scattered across the leaf surface, which is crucial in regulating gas exchange and water vapour loss. The distribution and density of stomata may vary depending on environmental factors such as light intensity, humidity, and carbon dioxide concentration [68,69].

The microstructure of the lower epidermis (E) of the Hazel (Corylus avellana L) leaf shows several important features that contribute to its function and adaptation to the environment. The lower epidermis consists of closely packed cells that form a protective layer covering the leaf surface. These cells appear flattened with thickened cell walls, providing the first layer of protection against drought, ultraviolet light, and pathogen attack [70].

A thorough analysis of the internal anatomy of Corylus avellana L. leaf shows intricate features essential for its physiological functions. Below the upper epidermis, the palisade mesophyll unfolds, showcasing elongated cells meticulously arranged

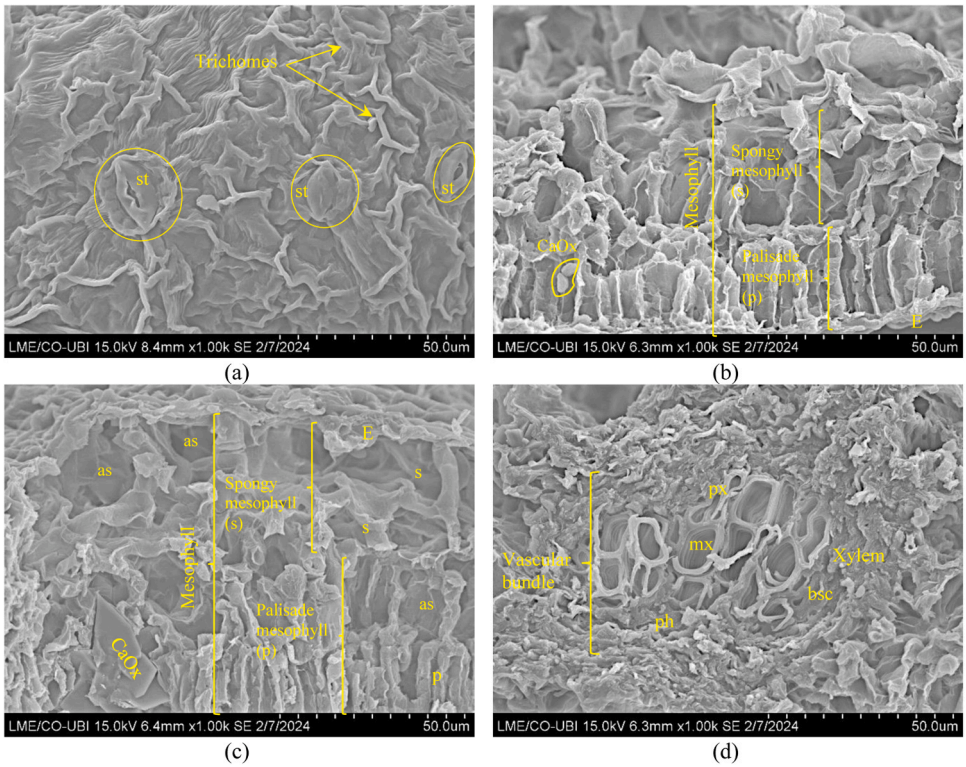

Fig. 6. SEM image of Hazel (Corylus avellana. L) Leaf in different positions. (a): Surface of the leaf; (b): Cross-section position of the leaf; (c): Cross-section position of the leaf with calcium oxalate crystals in the mesophyll; (d): Big vascular bundle. Abbreviations: (E) Upper and lower epidermis, Sz Guard cell; (P): Cells of the palisade parenchyma; (s): Cells of the spongy parenchyma, (as): air space; (ph): Phloem; (mx): Metaxylem; (px): Protoxylem; (bsc): Bundle sheath cells; (CaOx): calcium oxalate crystals.

perpendicular to the leaf surface. Additionally, the presence of spongy mesophyll below the upper epidermis. Adjacent to the palisade mesophyll resides the spongy mesophyll, featuring loosely packed cells interspersed with air spaces (as). This intricate arrangement facilitates efficient gas exchange, enabling carbon dioxide uptake and oxygen release during photosynthesis [71]. Furthermore, the mesophyll harbours a calcium oxalate crystal (CaOx), contributing to plant defence mechanisms against herbivory or serving as a reservoir for calcium ions (Ca^{2+}) [72].

Fig. 6,d demonstrates a big vascular bundle comprising xylem and phloem tissues that transport water, nutrients, and organic compounds throughout the leaf. Xylem vessels ferry water and minerals from the roots to the leaf, while phloem (ph) conducts organic compounds, such as sugars, synthesised during photosynthesis to other plant parts. Enveloping the vascular bundles are bundle sheath cells (bsc), offering structural support and regulating the movement of substances into and out of the vascular tissues. The function of each composition in the leaf tree structure was described in detail in the previous sections (↱4.1.1.1.1 and ↱4.1.1.1.2).

4.1.1.2. EDS analysis of the tree leaves materials. The EDS analysis of the tree leaves near the AHN yields crucial information regarding environmental factors and potential interactions with the hornet nest. The analysis of elemental composition reveals significant disparities. Specifically, Hazel, Chestnut, and European nettle exhibit significantly higher carbon (C) content, with respective percentages of 61.44 wt%, 58.79 wt%, and 56.8 wt%. The slight discrepancy in the carbon (C) content implies potential variations in organic matter and photosynthetic activity among these tree species [73]. Moreover, these trees (Hazel, Chestnut, and European nettle) stand out with notably higher oxygen (O) content, at 38.05 wt%, 36.63 wt%, and 39.96 wt%, respectively. This variation in oxygen concentration can likely be attributed to potential disparities in structural components such as cellulose and hemicellulose present in these tree species. The oxygen content in the chemical composition of leaves is influenced by the intricate interplay of various biochemical processes, including photosynthesis and the synthesis of different organic compounds such as cellulose, starch, and various secondary metabolites, which can vary among plant species [74]. Further, Magnesium (Mg), an essential element for photosynthesis and enzyme function [75,76], is present in Hazel (0.41 wt%) and European nettle (0.14 wt%), but not detectable in Chestnut. The low levels of aluminium (0.15 wt%) and silicon (0.25 wt%) in Hazel may indicate environmental exposure, while Chestnut and European nettle show undetectable levels of these elements. Phosphorus content shows a slight increase in Hazel (0.22 wt%) compared to Chestnut (0.2 wt%) and European nettle (0.14 wt%), may indicating potential differences in energy transfer processes observed across the analysed three tree species. The highest potassium concentration is found in the Chestnut (1.24 wt%), which is important for water regulation and activation of plant enzymes. Furthermore, calcium (Ca), essential for cell structure and signalling [77,78], is most

prevalent in European nettle (1.45 wt%). Hazel and Chestnut exhibit minimal presence of iron (Fe) and copper (Cu), proposing a potential difference in metal absorption capacity or environmental exposure [79]. Sulphur content is detected in Chestnut (0.13 wt%) and European nettle (0.11 wt%), while not detected in Hazel. The EDS analyses of the three tree leaves focus on the complex variations in elemental composition within these tree species.

4.1.2. SEM-EDS analysis of the tree leaves ashes

4.1.2.1. SEM analysis of the tree leaves ashes. Even following the combustion and transformation of the leaf into ash, some aspects of the leaf's physical structure and internal makeup seem to endure in the resulting ash. This persistence indicates that the ash could potentially maintain essential features of the original leaf's structure.

4.1.2.1.1. European nettle tree (Celtis australis) leaf ash. Fig. 7 presents the SEM image of the European nettle tree (Celtis australis) leaf ash, displaying the morphology of the altered leaf structure following incineration. The undulating morphology, reminiscent of rolling hills, clearly illustrates the significant damage inflicted upon the leaf during incineration. Moreover, areas exhibiting a heterogeneous morphology are apparent, marked by numerous voids of varying sizes. The SEM image reveals a highly porous microstructure, with interconnected pores contributing to the formation of a spongy network, thereby enhancing the complexity of the overall structure of the leaf ash. However, it is imperative to acknowledge the limitations of this SEM image in identifying the individual components of the leaf anatomy. The extensive damage sustained by the leaf obscures the distinct features that would typically facilitate such identification.

4.1.2.1.2. Castanea sativa Mill – The European Chestnut leaf (CSM-ECL) ash. The microstructure of Castanea sativa Mill – The European Chestnut leaf (CSM-ECL) ash, observed through SEM in Fig. 8, shows two distinct morphologies with a captivating complexity. Multi-uniseriate needle-shaped structures surround a substance that is even more intricate at the microscopic level. This sophisticated arrangement is crafted from an array of geometric and irregular shapes, forming a complex shape. The SEM image of the ash from the CSM-ECL shows a distinctive midrib and non-glandular trichomes uniseriate structure observed on the epidermal surface. The non-glandular trichomes observed on the epidermal surface of CSM-ECL ashes exhibit similarities to those detailed in the SEM images of Rubus idaeus L. leaves in the study conducted by Mirosława Chwil1 & Mikołaj Kostryco1 [52]. These trichomes, discernible in the SEM image, appear as elongated structures protruding from the leaf's epidermis. The distinctive presence of non-glandular trichomes [80,81]. In the SEM image, these non-glandular trichomes appear as elongated structures emerging from the leaf surface, exhibiting a discernible morphology. The non-glandular trichomes observed on the surface of CSM-ECL leaves in the SEM image (Fig. 8a) appear to be hair-like structures characterised by their slender and elongated shape. Their presence is notable across the leaf surface, demonstrating the widespread distribution of these trichomes.

The midrib shown in Fig. 8b, a central structural component of the leaf, exhibits noticeable damage. Within this impaired midrib, various components are discernible, contributing to a complex composition. The SEM image reveals the presence of a xylem network, phloem, fibres, and collenchyma tissue within the midrib. The xylem network, responsible for water transport, and the phloem, responsible for nutrient transport, are integral parts of the vascular system. Additionally, fibres, providing structural support, and collenchyma tissue, offering flexibility and reinforcement, contribute to the overall architecture of the midrib [82–84]. However, a noteworthy observation is that the phloem, fibres, and collenchyma tissue within the midrib appear significantly damaged. The SEM image shows the damage as these components have lost their original shape and morphology. The once distinct and organised structures of the phloem, fibres, and collenchyma tissue have undergone alterations, likely due to the ashing process.

The SEM image of CSM-ECL ash represents a notable presence of calciphytoliths, specifically calcium oxalate crystals (Fig. 8b), in the form of scattered prisms and clusters. This observation aligns with findings reported in previous studies [85,86].

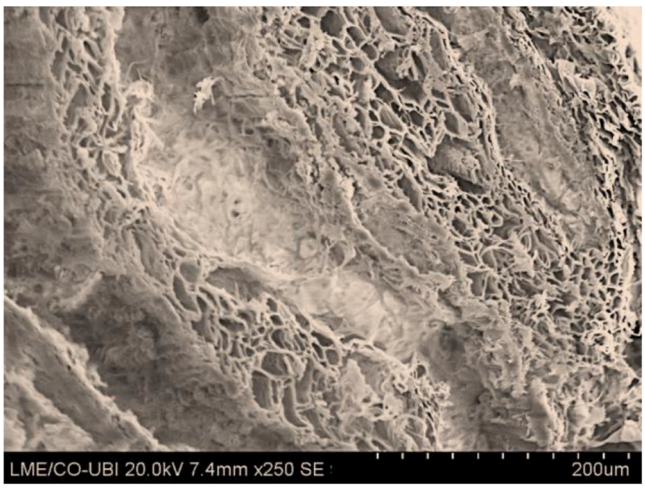

Fig. 7. European nettle tree (Celtis australis) leaf ash.

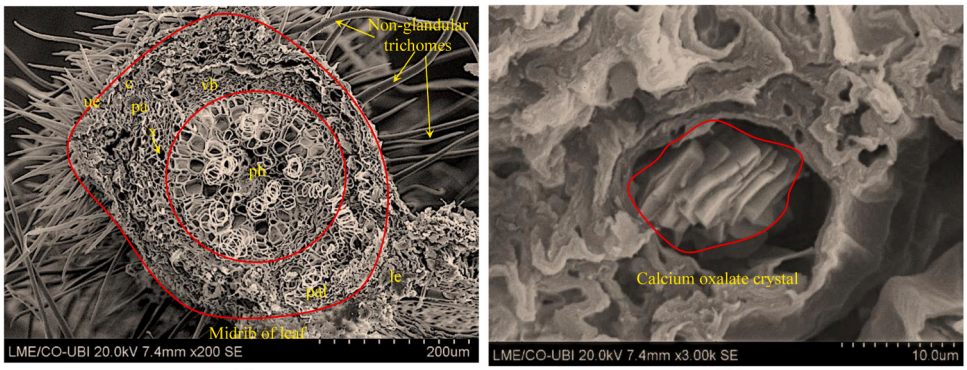

Fig. 8. Castanea sativa Mill – The European Chestnut leaf ash, b)- SEM image of the calcium oxalate crystal into midrib parenchyma cell. Abbreviations: ue = upper epidermis, c = collenchyma, pa = parenchyma, vb = vascular bundles, ph = phloem, x = xylem, pal = palisade, le = lower epidermis.

Fig. 8b presents a detailed visual representation of the non-organic material present in the leaf ashes. Calciphytoliths, characterised by calcium oxalate crystals, manifest as scattered prisms and clusters, showcasing a distinct and discernible structure. These non-organic elements are prominently distributed throughout the ashes remains of CSM-ECL leaves, indicating a significant proportion of inorganic content within the sample. Calcium oxalate crystals in leaves have been studied in various plant species. The crystals have specific geometric shapes and are formed in crystal idioblast cells. They serve multiple functions: calcium storage, carbon source, and metal detoxification. The crystals can be found in different leaf parts, including the mesophyll, vascular bundles, and aerenchyma. They have different shapes, including druses, prisms, and raphides. The size and density of the crystals can vary depending on the species and the environment [87–90]. Prismatic calcium oxalate (CaOx) crystals in tree leaves are produced through a specific developmental process. The formation of prismatic crystals initiates in the subapical mid-mesophyll layer of the leaf and then progresses basipetal, with additional prisms forming in the enlarging lamina. A pre-emptive wave of small prisms also appears basipetal in the midrib. These early-formed prisms expand vertically and eventually extend from the epidermis to the epidermis. Later-formed prisms attain intermediate sizes [91].

4.1.2.1.3. Hazel (Corylus avellana. L) leaf ash. The SEM image of Hazel (Corylus avellana L.) leaf ash in Fig. 9 presents a comprehensive view of the different components of the leaf residues. It shows a prominent vascular bundle surrounded by leaflets amidst many irregularly shaped thin particles reminiscent of delicately arranged slices. Analogous to the comparative Fig. 6d (before incineration), this image accentuates the uniform morphology of hazel leaf ash. Nevertheless, beyond its obvious similarity, this SEM image also reveals structural damage affecting key components of the leaf anatomy. Both the upper and lower layers of the epidermis exhibit noticeable compromise, possibly indicating degradation caused by the leaf incineration. Furthermore, significantly altered the shape of mesophyll, comprising both spongy and palisade mesophyll.

4.1.2.2. EDS analysis of the tree leaves ashes. Table 2 and Fig. 10 presents a detailed overview of the chemical composition of leaf ashes

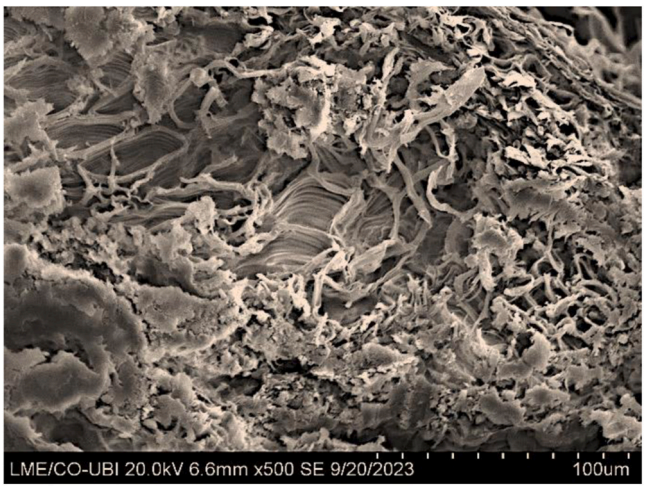

Fig. 9. Hazel (Corylus avellana L.) leaf ash.

derived from three distinct tree species investigated in this study: Corylus avellana (hazel), CSM-ECL, and European nettle, displayed in atomic percentages. The EDS analysis of the three leaves ashes demonstrates significant differences in the elemental makeup among these tree species.

The European nettle tree (Celtis australis) exhibits a notably high percentage of calcium (36.39 wt%), along with a moderate amount of potassium (9.42 wt%) and magnesium (4.61 wt%). However, Castanea sativa Mill – The European Chestnut demonstrates a convergent percentage of calcium (19.17 wt%) and potassium (18.33 wt%), accompanied by moderate levels of phosphorus (7.95 wt %), magnesium (3.94 wt%), and sodium (2.67 wt%). Additionally, Hazel (Corylus avellana. L) stands out with its high calcium content (31.44 wt%) and moderate amounts of phosphorus (2.36 wt%), magnesium (2.67 wt%), and silicon (5.58 wt%). In contrast, Hazel (Corylus avellana. L) shows the lowest levels of aluminium (0.15 wt%) and sulphur (0.81 wt%) compared to the other two species. While these variations are essential for understanding the nutritional characteristics specific to each tree, they also have implications for their ecological functions, such as nutrient cycling in soil ecosystems. This illustrates how diverse these tree species are in their respective environments. The role of each chemical composition element within the leaf anatomy and function is thoroughly detailed in section ↱4.1.1.2, giving a comprehensive understanding of their significance.

4.2. SEM-EDS analysis of the Asian hornet nest paper-like material

4.2.1. SEM-EDS analysis of the Asian hornet nest paper-like material (raw materials)

4.2.1.1. SEM-EDS analysis of the AHN outer envelope paper-like material

4.2.1.1.1. SEM analysis of the AHN outer envelope paper-like material. As demonstrated in Fig. 11, the outer envelope of the AHN is primarily constructed with tiny fragments of plant materials derived from sieve tubes or vessels from plant tissues and combined with the hornet's oral secretions to create a paper-like material [92]. This material is used to build the outer envelope regardless of the colour of the AHN P-LM, either strains or light. The air inside the nest experiences a decrease in temperature during the night, causing its humidity to increase. Consequently, some vapour in the outer envelope regions may condense [93]. Thus, the surface of the outer envelope is uniform with a light brown hue and has numerous minuscule pores, believed to regulate the temperature and humidity within the nest. The outer envelope SEM images identified and marked multiple regions of interest.

In the SEM image, region of Interest 1 (ROI: 1) presents etching in bordered pits at tracheid surfaces [94]. Bordered pits are microscopic structures in plant cells, specifically in tracheids or vessels of wood, playing a role in water transport and communication between adjacent cells [95]. Further, tracheids are elongated, tapering cells in the xylem of vascular plants that transport water and minerals. The surface of the tracheid is where the bordered pits are located [96]. Etching in this context (ROI 1) likely refers to removing or altering material on the surface of these bordered pits at tracheids. The etching phenomena identified within the bordered pits on tracheid surfaces indicate a potential involvement of hornets, leading to consequential alterations in wood anatomy, specifically within the tracheids. The etching in the bordered pits on tracheids within ROI: 1 indicates a plausible association with hornets' activity. It is proposed that hornets may have actively chewed through the bordered pits at the tracheid surface, contributing to discernible changes in overall wood structure. This observation prompts further consideration of ecological interactions between hornets and wood anatomy, emphasising the significance of such studies in understanding nuanced dynamics within ecological systems.

The SEM image's region of Interest 2 (ROI: 2) may correspond to distinct plant compositions, such as damaged mesophyll cells or midrib structures [82], characterised by a complex-shaped microstructure. Moreover, (ROI: 2) also exhibits the shape of the microscopic structure of a damaged vascular bundle [97]. This damage is likely a result of the hornets' chewing on the midrib and mesophyll cells of the plant's leaves. The shape of (ROI: 2) closely resembles the anatomy of leaf structures shown in Figs. 5d and 8a. In a thorough study of the microstructure aspect of the AHN P-LM, SEM images show the presence of palisade parenchyma mesophyll cells and bundle sheath strands in the outer envelope of the AHN P-LM. These two components are the main constituents of the tree leaf's structure, as analysed in Section 4.1.

Region of Interest 3 (ROI: 3) demonstrates the cellular features of vein bundle sheath cells of tree leaves [98], which are unique

Table 2
Chemical composition of the trees leaves ashes.

Element	Weight percentage (wt%)		
	European nettle tree (Celtis australis)	Castanea sativa Mill – The European Chestnut	Hazel (Corylus avellana. L)
Carbon	2.84	2.25	2.68
Oxygen	38.71	40.86	41.63
Sodium	0.65	2.67	2.42
Magnesium	4.61	3.94	2.67
Aluminium	0.20	0.32	0.15
Silicon	1.92	0.24	5.58
Phosphorus	3.60	7.95	2.36
Sulphur	1.44	2.76	0.81
Potassium	9.42	18.33	10.02
Calcium	36.39	19.17	31.44
Manganese	0.22	1.25	0.24

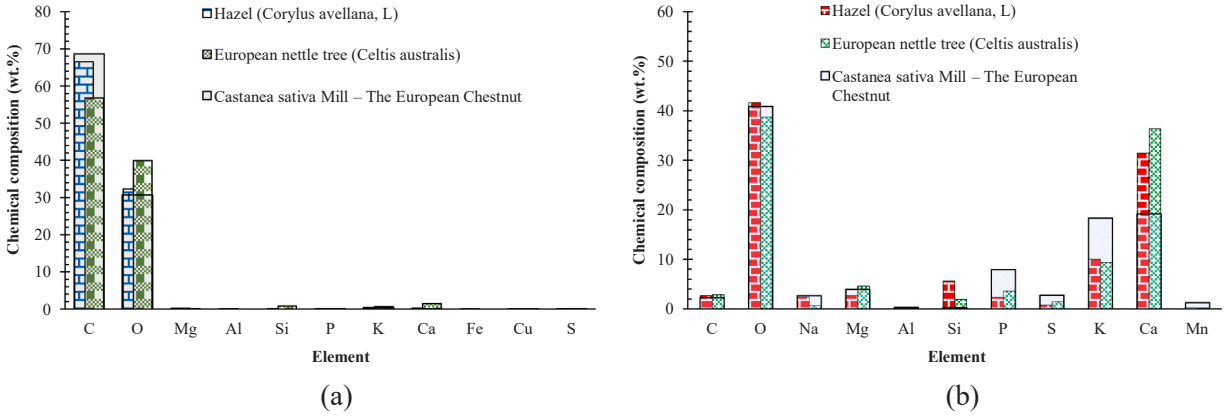

Fig. 10. Chemical composition of: (a) natural tree leaves (before inceneration) and, (b) leaves ashes.

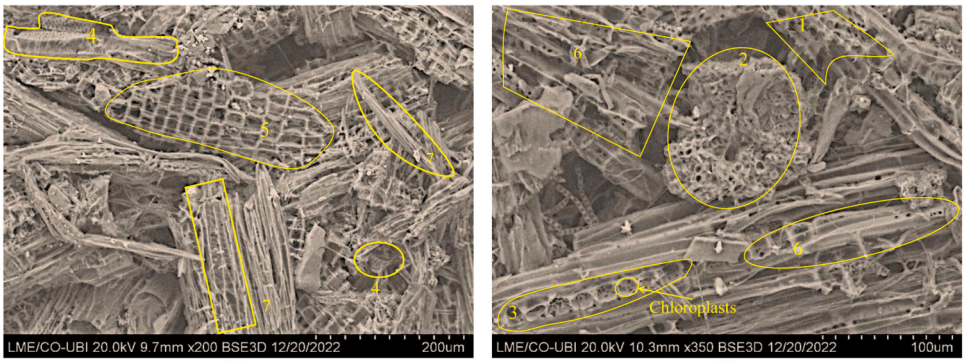

Fig. 11. SEM images of the piece taken from the outer envelope AHN P-LM.

photosynthetic cells primarily located in the leaves of C4 plants. They envelop the vascular bundles and are crucial in enabling the C4 photosynthetic pathway, contributing significantly to plant physiology and carbon assimilation [99]. Despite having a small chloroplast compartment, the bundle sheath cells exhibit substantial gene expression related to photosynthesis [100]. Moreover, the thick-walled bundle sheath cells contain large chloroplasts that lack granular stacking and are arranged centrifugally in the cell [101]. These chloroplasts have a different arrangement of thylakoids than those in mesophyll cells, and they are specifically adapted to facilitate the initial carbon fixation and the subsequent Calvin cycle [102–104]. G. Edwards and C. Black [105] have documented the presence of bundle sheath strands in crabgrass leaves. This observation implies that the hornets might have incorporated crabgrass leaves into their construction processes.

Region of Interest 4 (ROI: 4), represents a complex array of various shapes and sizes within the outer envelope of paper-like material. These shapes correspond to specific groups of wood components, such as the cell walls of axial or vertical early wood tracheids with bordered pits [106,107], as well as vessel pits or multi-pit membranes in wood anatomy [108,109].

The microstructural geometric shape and morphology of (ROI: 5) closely resemble the cellular structure of softwood, including transversal parenchyma tissue, collenchyma, and sclerenchyma cells. Parenchyma tissue forms the softer parts of plants and serves as filler tissue for stems and leaves, with the capacity for photosynthesis. In contrast, sclerenchyma tissue provides structural support in plants due to its thick, lignified cell walls, which make it hard and brittle at maturity. Collenchyma cells exhibit a structure that falls between these two types of ground tissues [110–113]. While elongated cells in (ROI: 5) show similarities with bundle sheath cells characterised by broader alternating with narrower cells, storage parenchyma contains wrinkled cell walls and plasmodesma fields within them. The microstructure of (ROI: 5) is comparable to the cellular structure of softwood, specifically resembling parenchyma, collenchyma, and sclerenchyma cells [114]. Furthermore, (ROI: 6) shows longitudinal earlywood tracheids; these tracheids exhibit distinctive features, notably bordered pits discernible in both the radial and tangential walls [110,115,116]. In addition, the (ROI: 7) appears to exhibit characteristics indicative of several potential features. It may correspond to fibre tracheids [117], elongated cells that transport water and nutrients throughout the plant. Alternatively, (ROI: 7) could represent the membrane [109], a thin layer that separates adjacent cells in plant tissues. Another possibility is that (ROI: 8) is associated with vessel elements [109].

Fig. 11 shows that thread-like structures may correspond to the oral secretion of hornets. This adhesive secretion holds the granules together within the tissue of tree wood and the different tiny fragments of plant material, resembling vegetable chips derived from

sieve tubes or vessels from plant tissue, allowing for the formation of the unique and robust hornet nest structure. The surface of the outer envelope has grooves, which are used to manipulate and apply the plant fibres. The grooves also help to increase the surface area and reduce the weight of the envelope. The outer envelope has numerous pores that allow gas exchange, temperature regulation and humidity control within the nest. The pores are distributed unevenly across the surface of the paper-like material.

Examining SEM images leads to results that indicate a uniform microstructure characterised by the intricate assembly and positioning of diverse elements such as plant fragments, tree leaves, and wood components within the AHN P-LM. The disordered orientation of plant fragments, tree leaves, and wood components in multiple directions emphasises the complexity and dynamism process involved in constructing this elaborate structure. This complexity can be attributed to multiple factors, including the coordinated efforts of numerous Asian hornets working simultaneously at a shared location. Their collaborative gathering of building materials from diverse sources results in a richly textured nest with an array of plant materials, showcasing their resourcefulness and adaptability.

4.2.1.2. Inorganic matter in AHN outer envelope P-LM (SEM-EDS analyses). During the SEM-EDS analysis, a specific region within the P-LM of the AHN outer envelope attracted attention due to its distinctive appearance, as illustrated in Fig. 12. This area exhibited a notable morphology and shape, vividly illustrated in the SEM image, revealing an organised assembly of cuboidal crystal grains ensconced within a tissue fibre matrix. The arrangement of these crystals was strikingly parallel and well-coordinated. The cuboid-shaped Ca-oxalate crystals observed in Fig. 12 closely resembled the shape and morphology of prismatic Ca-oxalate crystals found in the petiole tissues of nickel hyperaccumulators Rinorea cf. bengalensis and Rinorea cf. javanica (Violaceae) from Sabah, Borneo, as meticulously documented by Antony van der Ent et al. [118]. This interesting similarity indicates a potential association between the crystal microstructures found in the AHN and those documented in specific plant species. Moreover, prismatic calcium oxalate crystals have been observed not just in the bark tissue [119,120] but also in the depressions of axial tracheids and calcium oxalate crystals [107]. This wide range of occurrences implies a subtle relationship between the AHN and various plant-derived materials.

Prismatic calcium oxalate crystals have been observed in the petiole tissues of tree leaves [90]. These crystals form in the subapical mid-mesophyll layer of the leaf, with additional prismatic developing basipetal in the enlarging lamina [121]. Sometimes, a pre-emptive wave of small prismatic appears basipetal in the midrib [122]. The prismatic crystals produced early in leaf development can eventually extend from the epidermis to the epidermis [123]. It has also been observed that druses, another type of calcium oxalate crystal, form secondarily acropetally in the petiole and midrib [124]. These findings show that prismatic calcium oxalate crystals are present in the petiole tissues of tree leaves, along with other types of calcium oxalate crystals such as druses.

The values in Table 3 correspond to the analysis of the chemical elements of the total area shown in Fig. 12(a), which means it is a general analysis of the image. Making the mapping, it was found that carbon and oxygen are uniformly distributed, while calcium is concentrated in several points as seen in Fig. 12(b). A significantly increased calcium level was observed within this specified region, corresponding to a mass ratio of 22.84 %. This considerable accumulation of calcium indicates the existence of prismatic Ca-oxalate crystals, thereby augmenting our understanding of the microstructure. This indicates that hornets may have utilised leaf litter, comprising deceased plant material fallen from trees, shrubs, and other vegetation, for constructing their nests, which adds depth to the interpretation. This aligns with observed behaviours in the animal kingdom, where species exhibit a discerning preference for specific materials when constructing their habitats.

4.2.1.3. SEM-EDS analysis of wall cells of the AHN combs

4.2.1.3.1. SEM analysis of cells wall combs. Fig. 13 presents the scanning electron microscope (SEM) image of the paper-like substance that constitutes the comb in the AHN. Upon closer inspection of its microstructure, one can observe an enhanced homogeneity and denser material, as evidenced by the notable lack of discernible pores or identifiable plant fragments. Moreover, discernible attributes such as grooves, thin threads, and dispersed tiny granules become apparent. The thread-like structures may correspond to the oral secretion of hornets. This adhesive secretion acts as a mortar, effectively joining the plant materials. It serves as a

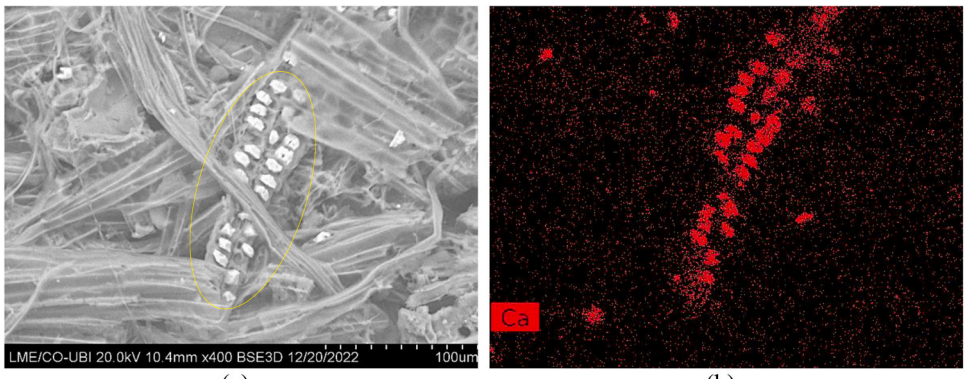

Fig. 12. (a) SEM image and (b) Elemental mapping analysis of a spot in the outer envelope of the AHN.

Table 3
Chemical composition of the spot in the outer envelope of the AHN.

Elements	Content (wt%)
C	25.75
O	51.41
Ca	22.84

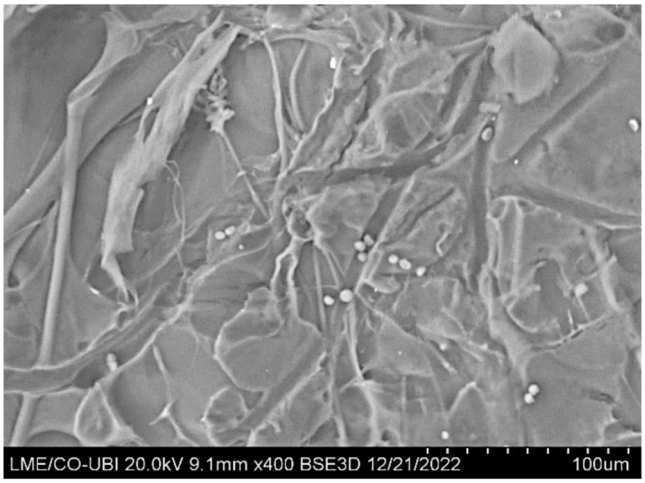

Fig. 13. SEM images of the Asian hornet's nest combs paper-like material.

unifying agent, orchestrating the cohesion of various plant elements within the nest. It seems that the Asian hornets engage in thoroughly chewing plant leaves, altering the plant materials' microstructure. Concurrently, during this intricate procedure, the hornets adeptly combine the chewed plant materials with their saliva. This dual action transforms the physical properties of the plant components and integrates them with the hornets' saliva, demonstrating a purposeful and sophisticated approach to dealing with plant raw materials for their nest's construction.

The P-LM of the combs in the AHN is mainly made up of plant fibres, which the hornets gather and chew to create a pulp-like substance. In contrast to the outer envelope, which often shows a more structured and organised appearance under SEM imaging Fig. 11, the material of the combs appears less defined and lacks specific shapes or patterns. This difference in appearance can be attributed to the processing the plant fibres undergo within the hornets' mandibles. When hornets collect plant fibres to build their nests, they mix them with saliva, chew them, and then regurgitate the resulting pulp onto the nest structure. This chewing and mixing process breaks down the fibres and blends them into a uniform material suitable for constructing the combs. Consequently, the fibres lose much of their original structure and may appear less distinct under SEM imaging than those in the outer envelope.

4.2.1.3.2. EDS analysis of cells wall combs P-LM. EDS analysis indicates that carbon (C) and oxygen (O) comprise 81.4 wt% of the nest cells' wall combs-like-paper material composition. This indicates that Vespa velutina nigrithorax mainly uses organic matter when constructing nests [125]. Among the organic materials were likely detritus and plant matter, commonly found in the natural environment. These compounds were found in section ↱4.1.1.2, which shows the SEM-EDS analysis of the tree leaves near the nest, such as the Chestnut leaves, European nettle leaves, and Hazel (Corylus avellana. L) leaves.

The EDS examination also identifies small amounts of additional elements like silicon, aluminium, calcium, magnesium, iron, sodium, and potassium. These may have come from soil particles or mineral dust binding to the plant fibres. This indicates that V. velutina nigrithorax can collect and use hydrocarbons from their environment to construct their nest. Which are common in the paper and organic materials used to construct the nest. It seems that V. velutina nigrithorax is well adapted to its environment and able to use the resources available. The presence of several inorganic elements, such as nitrogen (N), potassium (K), silicon (Si), magnesium (Mg), phosphorus (P), sulphur (S), chlorine (Cl), and aluminium (Al), which represent approximately 16.8 wt% of the composition, in an Asian hornet nest could indicate a variety of things about the nest material. The EDS analyses cannot conclude that Vespa velutina nigrithorax regularly collects mud and/or inorganic particles in the field because the possibility that such a material contaminated the plant materials is not excluded.

The construction and maintenance of nests by Vespa velutina nigrithorax (yellow-legged hornet) involves a significant amount of oral secretion from the workers. This is because yellow-legged hornets use a combination of oral secretions and wood fibres to form the nest material. Oral secretions provide the necessary stickiness to hold the fibres together and act as a binder to bind the nest materials together, providing structural strength and durability. EDS analyses reveal that the cell walls of the combs have a high nitrogen content (16.46 wt%), which indicates the presence of a high content of oral secretions. Nitrogen is essential for both hornets and plants, as it is

involved in various biological processes. Plants obtain nitrogen from the soil through nitrate absorption, which requires molybdenum as a catalyst. Molybdenum, a crucial element, facilitates the transformation of nitrate (NO^{3-}) into nitrite (NO^{2-}), a process that aids in nitrogen assimilation by plants [126,127]. Therefore, oral secretions and plant tissues contribute to the nitrogen content of the nest material.

4.2.1.4. SEM-EDS of AHN P-LM ash. The AHN P-LM sample was subjected to a two-hour (2 h) heating at 800 ºC to eliminate organic matter and examine potential minerals or inorganic compounds in the outer envelope. This method allowed for the elimination of organic matter, which decomposes at such high temperatures. Any inorganic compounds in the sample could then be analysed, as they can withstand the heat. The remaining material was analysed using EDS to reveal the inorganic chemical composition of the nest. Additionally, an XRD analysis was conducted on the burnt outer envelope sample of the AHN to identify any crystal phases present in the material. This allowed for the identification of mineral components and potential contaminants in the nest paper-like material. During the decomposition process at a temperature of 800 ºC for two hours, the organic matter undergoes thermal degradation, releasing volatile components such as water, carbon dioxide, and other gases. The remaining residue, known as ash, consists of the inorganic components present in the original material.

The burning process of the AHN P-LM releases heat, which causes the organic matter to break down. This process destroys the regular microstructure (geometric shapes and fibres) and transforms it into granules of varying shapes and sizes, as shown in Fig. 14,a.

While heating the AHN paper-like sample to a temperature of 800 ºC for two hours, a small quantity of carbon (C) remained in its chemical composition. Despite the intense heat and prolonged exposure, (2.36 wt%) of the carbon managed to withstand the thermal decomposition and remained within the resulting AHN paper-like material ash. The high calcium content (21 wt%) found in the AHN P-LM ash following decomposition indicates that the initial nest-building material had a substantial amount of calcium compounds in terms of inorganic matter. The presence of vegetable chips derived from sieve tubes or vessels from plant tissues and bark tissue from poplar wood suggests that the original plant material contained calcium-rich structures [106]. Sieve tubes and vessels are part of the vascular system in plants and are responsible for transporting water, nutrients, and minerals throughout the plant that contain calcium [88]. Poplar wood, a type of hardwood, typically contains higher levels of minerals than softwood [106]. Calcium is an essential plant nutrient and a common mineral found in many plant tissues [128], including bark tissue from poplar wood. Therefore, the combination of these plant fragments and the poplar wood bark tissue contributed to the high calcium content in the ashes of the paper-like material after decomposition at 800 ºC for two hours. The findings align with the visual representation of the SEM image (Fig. 12), indicating the existence of calcium cuboidal crystal grains. Calcium persists even after the sample undergoes combustion and transforms into ash.

Calcium (Ca) transport in the xylem occurs by mass flow of free Ca^{2+}, some organically complexed Ca, and chromatographic movement along Ca-exchange sites in the xylem walls. The delivery of Ca to transpiring leaves and weakly transpiring meristematic zones is discussed, as well as the two modes of Ca movement in the xylem. Competition between sinks is intensified when [Ca^{2+}] in the xylem is low and transpiration is great [129]. The presence of silica (Si) in the P-LM ash of the AHN is approximately (7.6 wt%). This silica content may originate from the cell walls and lumina of phytoliths in vascular plants [130–133].

The chemical composition of the three analysed leaves includes elements such as sodium (Na), potassium (K), and phosphorus (P) [134–137]. While the two alkali cations Na^{+} and K^{+} have similar relative abundances in the Earth's crust, they exhibit significantly different distributions in the biosphere [138]. Potassium, calcium, magnesium, and phosphorus are among the major elements present in leaves [139]. Phosphorus, following sodium, calcium, magnesium, and potassium in descending order, is also a significant element in leaves. The presence of these elements in leaves is crucial for plants' overall health and nutrient content.

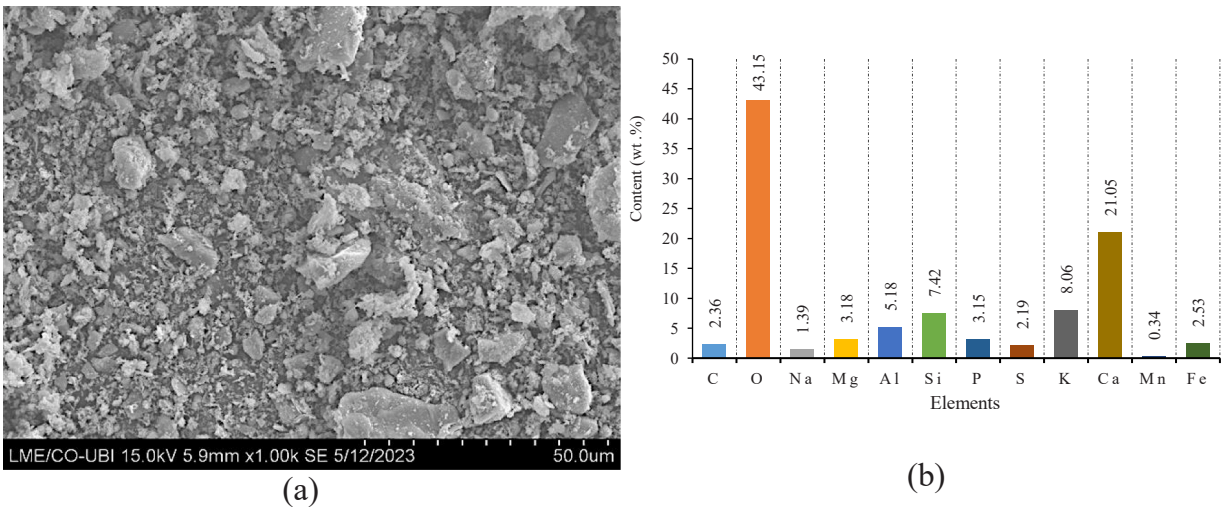

Fig. 14. SEM-EDS analysis of the AHN like-paper material ash, (a): AHN P-LM ash, and (b): EDS of the AHN P-LM ash.

4.2.2. The analysis of P-LM different colours in the outer envelope

4.2.2.1. SEM analysis of P-LM in the outer envelope of AHN. The AHN outer envelope consists of a paper-like material (P-LM) with multiple layers that exhibit diverse colours, ranging from light to dark shades. Fig. 15 shows a selected sample extracted from a section of the outer envelope of the AHN P-LM. Besides, SEM images obtained from diverse segments with distinct regions of interest are presented for a detailed analysis of the microstructure and morphology, revealing the factors contributing to the varied colours observed in the material. Within the SEM images, the colour representation is delineated across different Regions of Interest (ROI):

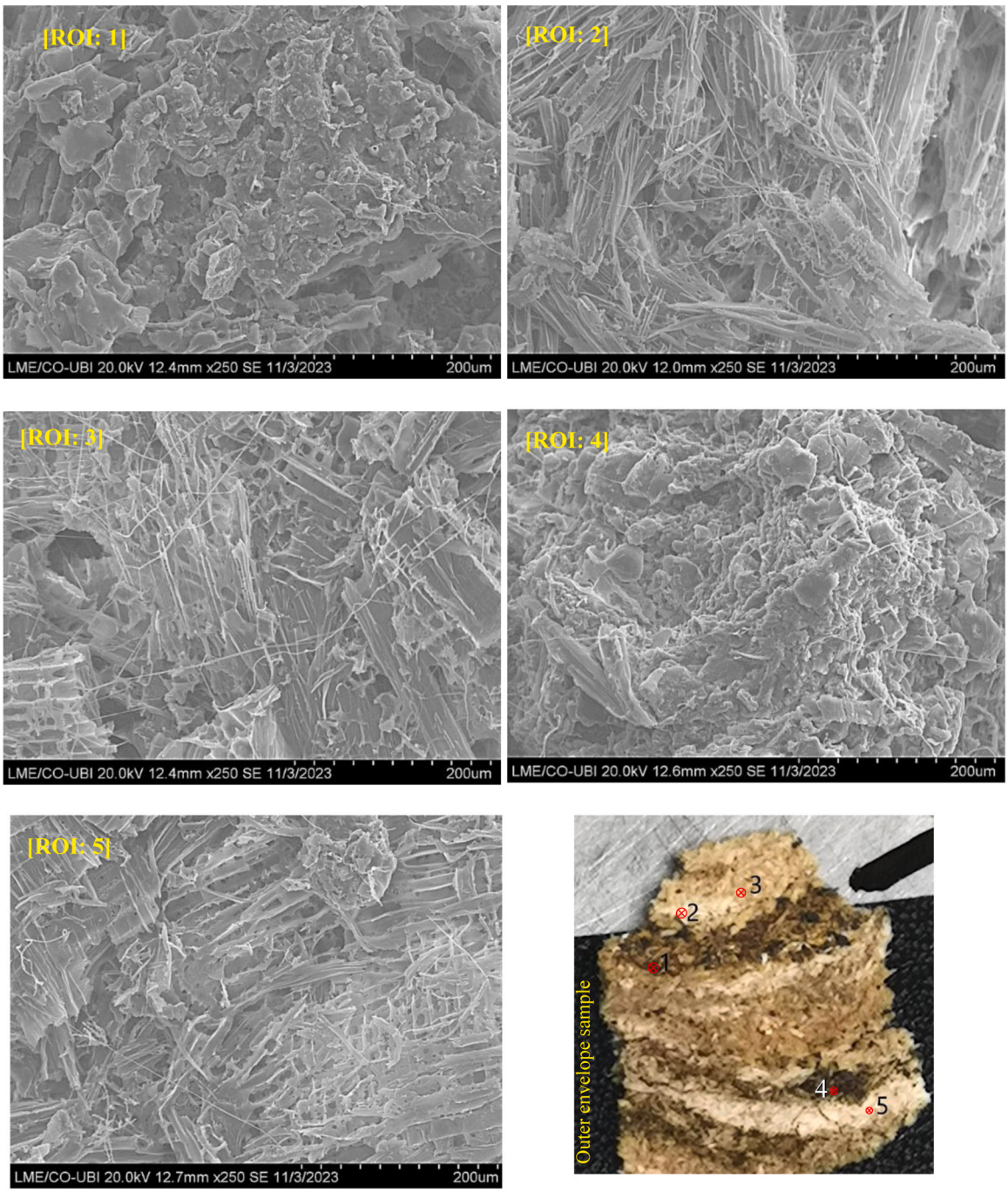

Fig. 15. Scanning electron microscope images of the AHN outer envelope: [ROI: 1] Iroko colour, [ROI: 2] Linen colour, [ROI: 3] Chamoisee colour, [ROI: 4] Dark Charcoal colour, and [ROI: 5] Cornsilk colour, showing the difference between the surface colours. The last image is the AHN outer envelope sample.

[ROI: 1] appears as Iroko colour (#47301 F), [ROI: 2] exhibits a Linen colour (#f2e4da), [ROI: 3] presents a Chamoisee colour (#A0785A), [ROI: 4] is characterised by a Dark Charcoal colour (#333333), and [ROI: 5] shows a Cornsilk colour (#fffbe0). Regions of interest (ROI: 2, ROI: 3, and ROI: 5) present a similar microstructural morphology. In these regions of interest, a diverse composition is observed, consisting of various fibres, fragments of plants, and delicate threads. This intricate network serves to interconnect and bind the plant fragments together. Upon closer examination using SEM, distinct morphological characteristics emerge within the specified dark regions of interest, specifically [ROI: 1 and ROI: 4]. An in-depth scrutiny of these areas reveals morphologies that markedly differ from those observed in the remaining regions of interest [ROI: 2, ROI: 3, and ROI: 5]. SEM images of the zones [ROI: 1 and ROI: 4] demonstrate an irregular morphology marked by a profusion of particles with a reduced number of interconnecting thread-like materials. This distinct feature implies a deviation from the more uniform and interconnected structure observed in Zones [ROI: 2, ROI: 3, and ROI: 5]. The decreased presence of thread-like materials and plant fragments in these regions indicate the variations in the composition or assembly processes of the materials used by the Asian hornets in constructing the nest. These differences contribute to the unique morphological attributes observed in the examined SEM images across various regions of the outer envelope specimen.

4.2.2.2. EDS analysis of P-LM in the outer envelope of AHN. The elemental compositions within the darkest zones [ROI: 1 and ROI: 4] is examined through the implementation of EDS analysis. The chemical composition is indicated by the distinct colours observed in [ROI: 1] (Iroko colour, #47301 f) and [ROI: 4] (Dark Charcoal colour, #333333) within the outer envelope of the AHN P-LM. The deeper shade in [ROI: 4], characterised by a higher carbon content, implies the presence of organic compounds or materials contributing to the profound hue. Conversely, the lighter colour in [ROI: 1], attributed to higher oxygen content, may signify differences in oxidation states or the prevalence of oxygen-rich compounds. The unique colouration of [ROI: 1] could be influenced by the significantly higher (Al) content, while the observed variations may be contributed by the elevated silicon content. The role of sulphur in influencing colour is showed by its presence in [ROI: 4] and its absence in [ROI: 1], along with the small amount of copper detected in [ROI: 1]. The distinct colours observed in different regions of the AHN's outer envelope are collectively contributed by these differences in chemical composition.

The deeper shade in [ROI: 4], characterised by a higher amount of carbon, shows the existence of organic compounds that contribute to the profound tone. On the other hand, the lighter colour in [ROI: 1], which is attributed to higher oxygen content, may indicate variances in oxidation states or oxygen-rich compounds. The markedly higher aluminium content and the presence of sulphur differentiate the distinct colouration between these strip areas of the outer envelope in the AHN P-LM. [ROI: 4] exhibits a slightly higher carbon (C) content (71.94 wt%), in contrast to [ROI: 1] with (68.82 wt%). The deeper strip colour in [ROI: 4] could be associated with a higher carbon content, indicating the presence of organic compounds or materials that contribute to the profound hue. Moreover, [ROI: 1] shows a higher oxygen (O) content (27.16 wt%) compared to [ROI: 4] with (25.07 wt%). The elevated oxygen content in [ROI: 1] might contribute to a lighter strip colour, potentially showing differences in the oxidation state or the presence of oxygen-rich compounds. [ROI: 1] exhibits a significantly higher aluminium (Al) content (1.6 wt%) compared to [ROI: 4] with (0.79 wt %). The distinct strip colour in [ROI: 1] could be associated with a higher concentration of aluminium compounds, potentially influencing the overall strip colouration. Additionally, [ROI: 1] reveals a higher silicon (Si) content (1.49 wt%) compared to [ROI: 4] with (0.82 wt%). Silicon compounds, known to impact colour, may contribute to the observed differences in colour between [ROI: 1] and [ROI: 4]. Furthermore, [ROI: 4] has a notable sulphur (S) content (0.54 wt%), while [ROI: 1] has none. The presence of sulphur in [ROI: 4] may be associated with specific compounds that contribute to the dark colour, while its absence in [ROI: 1] may influence the lighter colour. [ROI: 1] contains a small quantity of copper (Cu) (0.07 wt%), whereas [ROI: 4] has none. Even in small amounts, copper can influence the colour in [ROI: 1], possibly contributing to the overall Bistre hue. The EDS analysis of zones [ROI: 1] and [ROI: 4]

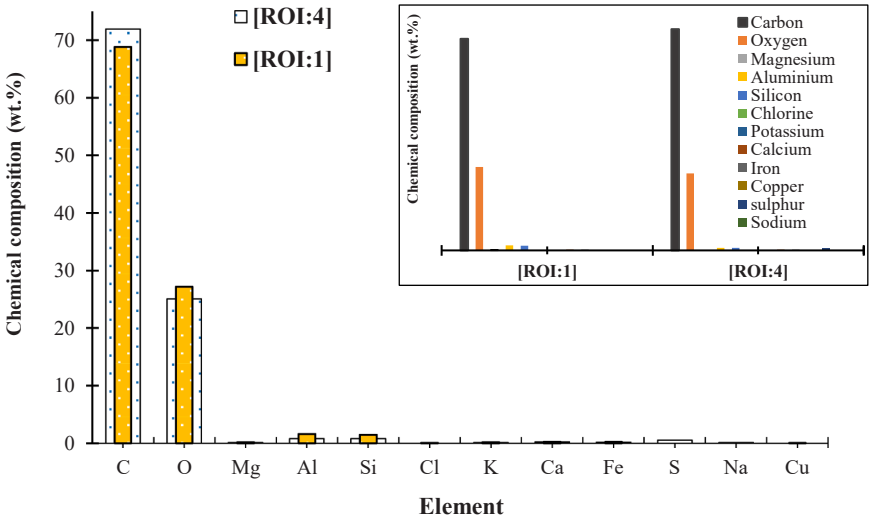

Fig. 16. EDS analysis of the AHN outer envelope P-LM different colours for zones [ROI: 1] and [ROI: 4].

shows that the colour differences between [ROI: 1] and [ROI: 4], possibly because of variations in the concentrations of specific elements, such as carbon, oxygen, aluminium, silicon, sulphur, and copper. These variances in chemical composition contribute to the unique colours observed in different regions of the outer envelope of the AHN.

4.3. XRD analysis

X-ray diffraction patterns were conducted on four ash samples obtained from the leaves of three distinct tree species and the paper-like material found in an Asian hornet nest. The resulting patterns can be seen in Fig. 17. Peak identification in the XRD patterns was carried out using Materials Data® MDI/JADE6 software, which compares experimental peak positions with a database of standard patterns, specifically utilising the Joint Committee on Powder Diffraction Standards (JCPDS, 2000) for mineral identification.

4.3.1. XRD analysis of the tree leaves ash

Fig. 17 (b, c and d) shows X-ray diffraction patterns results obtained from analysing tree leaves, namely the European Chestnut (Castanea sativa Mill), the European nettle tree, and Hazel ashes. The XRD pattern of the plant ashes (from the European nettle tree, Castanea sativa Mill, and Hazel (Corylus avellana. L) leaves ashes shows the presence of several compounds, including oxides, carbonates, and hydroxides of calcium (Ca), magnesium (Mg), and potassium (K). The XRD patterns obtained from the leaves' ashes showed a mostly amorphous composition, with various crystalline phases such as lime, phlogopite, microcline, calcium silicate,

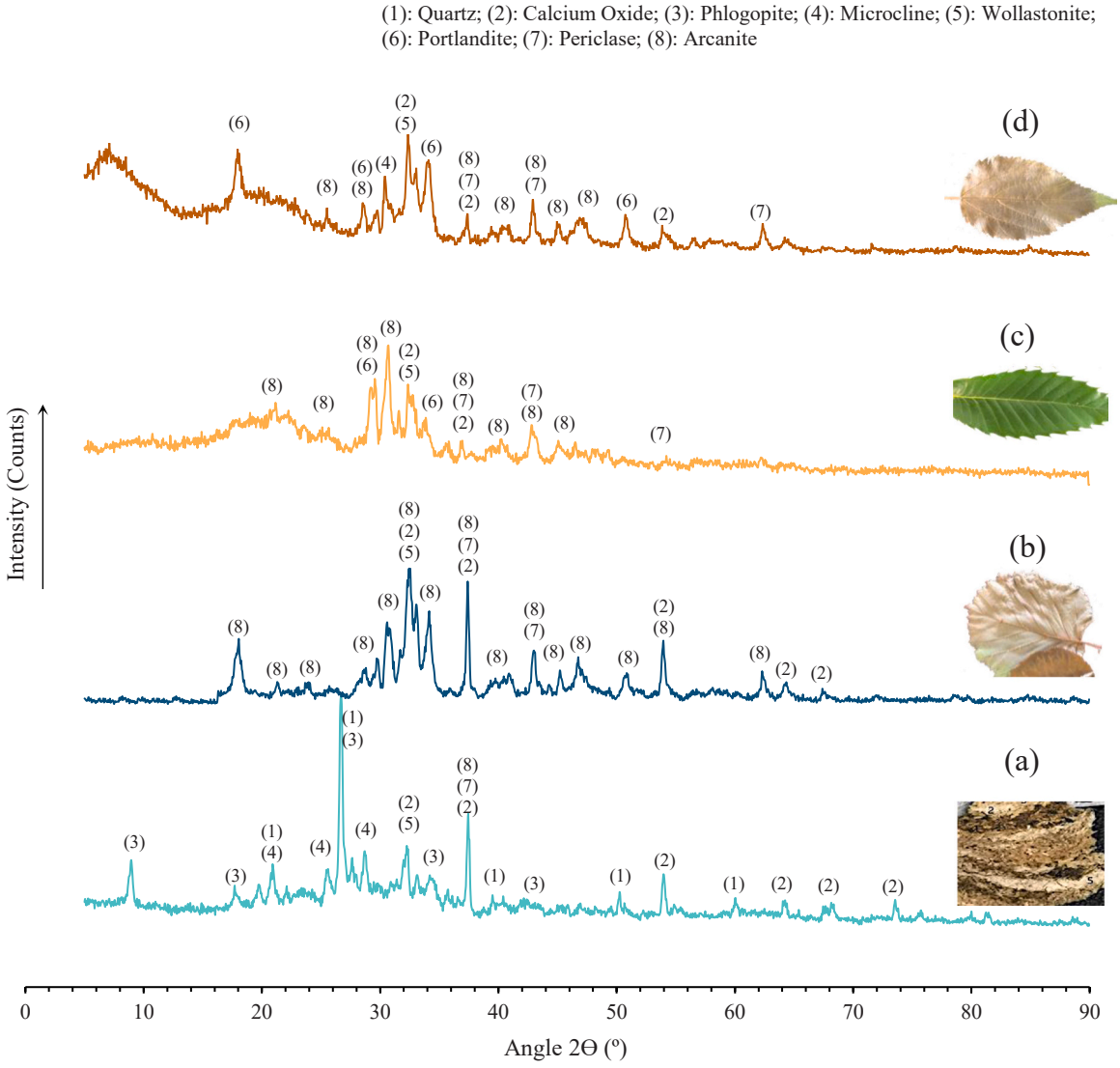

Fig. 17. XRD patterns and intensities of: (a)- AHN outer envelope P-LM, (b)- European nettle tree, (c)- Castanea sativa Mill, and (d)- Hazel (Corylus avellana. L) leaves.

portlandite, periclase, and arcanite. Upon in-depth analysis of the XRD patterns, lime (CaO) was identified in the ash patterns derived from three distinct leaves. Lime, as represented by the standard pattern number PDF#37–1497 (JCPDS, 2000), belongs to the lime-monteponite series and is characterised by an isometric crystal system. This particular mineral is notably observed in the ash of the leaves of the European nettle tree, where it exhibits noticeable peaks at angles of 32.5°, 37.4°, 54°, 64.05°, and 67.2° (2θ). Likewise, the ash of leaves from the Castanea sativa Mill tree also contains lime, which can be identified at angles of 32.5° and 37.4° (2θ). Similarly, the ash of Hazel (Corylus avellana. L) leaves exhibited a distinctive crystalline peak for the lime at angles of 32.5°, 37.4°, and 55° (2θ). The presence of lime in the ash patterns of these various leaves indicates a potential source from calcium oxalate (CaO_x) crystals within the leaf tissues. The lime peaks in the leaves ash XRD patterns confirm the calcium oxalate (CaO_x) crystals observed in the SEM images. Moreover, periclase (MgO) identification was based on the standard pattern number PDF#45–0946 (JCPDS, 2000), indicating its association with the periclase group characterised by an Isometric crystal system. The XRD patterns showed that periclase was present in all three tested leaves ashes. In the European nettle tree leaf ash pattern, distinct periclase crystalline peaks were observed at 37.35°, 43.15°, and 62.55° (2θ). Similarly, for the Castanea sativa Mill leaf ash pattern, sharp periclase crystalline peaks emerged at 37.35°, 42.8° and 54.15° (2θ). Hazel (Corylus avellana. L) leaf ash pattern exhibited two crystalline peaks at 37.35° and 43.15° (2θ). Ivana Carević et al. [140] detected Periclase in wood biomass ash. Furthermore, microcline ($K(AlSi_3O_8)$) was detected in the XRD pattern of Hazel (Corylus avellana. L) leaf ash at peak situated in angle (2θ) = 30.5°. Microcline was identified in the standard pattern number PDF#19–0926 (JCPDS, 2000), classified under the triclinic crystal system, and is a Feldspar (alkali) group member. It exhibits a prismatic crystal elongation along [001] or [100], reaching dimensions of up to 50 m and weighing approximately 13,500 t. Its morphology is granular and massive, commonly forming perthitic intergrowths [141]. Arcanite, also known as potassium sulfate (K_2SO_4), is a noticeable element in the ashes of the three analysed leaves. It has been identified with the standard pattern number PDF#05–0613 (JCPDS, 2000). Arcanite exhibits an Orthorhombic crystal system and belongs to the point Group: 2/m 2/m 2/m. It has a pseudo-hexagonal tablet shape, measuring up to 1 cm [141]. The mineral arcanite is commonly found in biomass ashes [142]. With the chemical formula (CaSiO3), Wollastonite is characterised by a monoclinic or triclinic crystal system. Its point group is either 2=m or 1. The wollastonite crystals are tabular, exhibiting faces labelled as f100g or f001g. Alternatively, they can also be short to long prismatic, reaching sizes up to 20 cm [141]. Wollastonite was detected in the XRD patterns of the three leaves ashes obtained from the European nettle tree and Hazel trees at specific Peaks: 32.45°, 32.35°, and 32.45° (2θ), respectively, indicating its presence in all three samples. In mineralogy, wollastonite has been observed in plant material, specifically in the mineralogy of bamboo leaf ashes [143]. The mineral Portlandite ($Ca(OH)_2$) exhibits a standard pattern number (PDF#44–1481) and possesses a Trigonal crystal system with a Hexagonal Point Group: $\bar{3}$ 2/m [141]. It manifests in hexagonal plates, attaining sizes of up to 6 cm. Portlandite has been identified in the leaves of Castanea sativa Mill and Hazel (Corylus avellana. L). In the XRD pattern of Hazel (Corylus avellana. L), Portlandite is discernible at 17.95°, 25.5°, 34.25°, and 50.7° (2θ). Conversely, in the XRD pattern of Castanea sativa Mill leaf ash, Portlandite is detected at angles (2θ) of 29.65° and 33.85°. Notably, Portlandite is conspicuously absent in the XRD pattern of the ash derived from the paper-like material of the Asian hornet nest. Additionally, periclase (MgO), lime (CaO), and portlandite ($Ca(OH)_2$) can be detected in wood ash [144].

4.3.2. XRD analysis of Asian hornet nest paper-like material ash

Fig. 17(a) presents the X-ray diffraction (XRD) patterns of the ash derived from the AHN P-LM. Through a comparison with standard patterns, it was ascertained that the XRD pattern of the AHN P-LM ash exhibited the presence of various minerals. The AHN P-LM ash pattern shows a mostly amorphous material with few crystalline phases including quartz (SiO_2) with the standard pattern number 46–1045 (JCPDS, 2000), lime (CaO) with standard pattern number 48–1467 (JCPDS, 2000), phlogopite ($KMg_3Si_3AlO_{10}(F; OH)_2$) with standard pattern number 10–0495 (JCPDS, 2000), and microcline ($KAlSi_3O_8$) with standard pattern number 19–0926 (JCPDS, 2000). These minerals were confirmed based on their respective standard pattern numbers. However, microcline was observed to have relatively low peak intensities. Notably, a distinct peak intensity was observed at 26.7° (2θ) in the AHN P-LM ash's XRD pattern, indicating quartz's presence. This distinctive feature was exclusively observed in the paper-like material of the AHN. Another peak corresponding to quartz was also detected at 60.65° (2θ). Quartz, a mineral commonly identified as rock crystal, is frequently encountered within geological formations and terrestrial sediment [145,146]. Furthermore, the incineration of agricultural residues has the potential to induce a metamorphosis in quartz, resulting in its conversion into amorphous silica, subsequently undergoing a process of crystallisation (taking on a crystalline structure) to form cristobalite [147–149]. Thus, the presence of quartz in the AHN P-LM ash indicates that it originates from the incineration of the AHN P-LM, which contain agricultural substances. The presence of calcium oxide in the AHN P-LM ash was confirmed at specific angles (2θ): 32.1°, 37.5°, 54.05°, 64.5°, 68.2°, 73.8°, and 81.8°. Importantly, calcium oxide has also been detected in the XRD patterns of leaf ashes, as mentioned in section ↱↱4.3.1. This indicates that (CaO) mineral originates from calcium oxalate (CaOx) crystals, particularly in leaf tissue. Phlogopite, belonging to the Mica group, possesses a monoclinic crystal system with the chemical formula ($KMg_3Si_3AlO_{10}(F; OH)_2$). Phlogopite is identified by standard pattern number PDF#10–0459. The phlogopite was found in the XRD patterns of the AHN P-LM ash at the following peak angles (2θ): 8.95°, 26.7°, and 34.2°. The presence of Microcline ($KAlSi_3O_8$) in the X-ray diffraction pattern of the AHN P-LM ash obtained from the paper-like substance that constitutes the AHN shows significant similarity to the mineral composition of wood ash [150]. These results strongly indicate a possible link between the mineral content present in material from AHN's and that found in wood ash. This connection leads to interesting speculation that Asian hornets used wood to construct and build their nest. The shared existence of Microcline, a mineral often linked with wood combustion (burning), further supports this suggestion. A single peak of the Wollastonite mineral is detected at an angle of (2θ) = 23.2° in the AHN P-LM ash sample. Furthermore, based on the identification of wollastonite in the ash of leaves, it is apparent that this mineral has the potential source from the leaf's ash for the P-LM that constitutes the AHN. The peak observed at (2θ) = 23.2° in the XRD pattern of the AHN P-LM ash sample closely resembles the peak found in the

ash of European nettle tree leaves, particularly in peak width and intensity. This specific peak corresponds to minerals such as calcium oxide, arcanite, and periclase. Interestingly, a similar peak is also evident in the XRD patterns of Castanea sativa Mill, and Hazel (Corylus avellana. L) leaves ash; nevertheless, in these cases, the peak intensity is comparatively lower. The aforementioned findings indicate that the mineral composition exhibited in the AHN P-LM ash of the Asian hornet exhibits resemblances to the composition found in rocks and soil, as well as in wood ash and leaves ash.

5. Replicate the AHN paper-like materials with the biomimicry concept

To replicate the AHN P-LM, one must apply the biomimicry concept, drawing inspiration from nature to develop innovative solutions for various challenges. In the civil engineering field, many studies have been conducted on biomimicry approaches to enhance sustainability, efficiency, and resilience in civil engineering projects by harnessing nature's wisdom [24,29,151–155].

The biomimicry of the AHN P-LM represents a significant example of biomimicry in civil engineering, serving as a preliminary study towards sustainability by paving the way for eco-friendly building materials. Biomimicry of the Asian hornet nest involves studying the intricate structure and materials used by Asian hornets in nest construction and applying these principles to engineering design and construction, as shown in Fig. 18. The architecture of the Asian hornet nest, characterised by its intricate hexagonal cells and multi-layered structure, inspires efficient and lightweight construction techniques. Emulating these design principles can lead to innovative building systems that optimise material usage and structural performance. Furthermore, in the biomimicry of the AHN P-LM, researchers first need to apply the knowledge gained from a comprehensive understanding of the biological and natural processes involved in nest building. Currently, the biomimicry of the AHN P-LM is in its initial stage, focusing on understanding the biological and natural processes involved. Additionally, the thermal regulation mechanisms employed by Asian hornets to maintain optimal conditions within the nest can inspire the development of energy-efficient building systems for heating and cooling.

A systematic approach can be adopted to replicate the AHN P-LM, divided into two key steps. In Step 1, a comprehensive understanding of biological and natural processes is pursued through detailed examination, segmented into three parts. Firstly, the thorough analysis of raw materials involves meticulously scrutinising the chemical composition, microstructure, mineralogy, and structural bonding of plant materials used in nest construction. Various techniques such as SEM-EDS, XRD, TG-DTG, and FTIR are employed to accomplish this scrutiny. Secondly, the in-depth examination of hornet behaviour focuses on understanding the behaviour of Asian hornets, particularly their involvement in nest construction. Special attention is given to deciphering the chemical composition of hornet saliva and studying their manipulation of raw materials through chewing. Lastly, the detailed characterisation of nest material involves analysing the paper-like material that makes up the Asian hornet nest using similar analytical techniques as in the previous phases. The chemical composition, microstructure, mineralogy, and bonding properties are scrutinised to gain insights into its structure and integrity. In Step 2, the application of biomimicry principles enhances the replication of the AHN P-LM, resulting in building materials that are more sustainable, efficient, and resilient. These principles include:

1. Emulate nature: Study natural systems to understand their approaches to problem-solving.
2. Sustainability: Creating eco-friendly solutions in alignment with natural ecosystems.
3. Efficiency: Imitate the optimised designs found in nature for more effective human systems.
4. Adaptation: Incorporate nature's resilience to adapt to changing conditions.
5. Integration: Collaborate across various fields to create and develop innovative solutions.
6. Life-friendly chemistry: Prioritise non-toxic, non-harmful, biodegradable materials and processes.
7. Feedback loops: Implement natural feedback mechanisms for system optimisation.
8. Resilience: Design systems capable of withstanding disturbances and recovery.
9. Cradle-to-Cradle Design: Aim for product and material reuse, recycling, or return to nature.
10. Innovation through diversity: Draw inspiration from nature's diverse strategies for problem-solving.

6. Outlook of biomimicry, the Asian hornet nest paper-like material in civil engineering

In the future, drawing inspiration from biomimicry could lead to the development of materials based on the AHN P-LM. These materials could be advanced building materials, providing coating films with exceptional surface dryness and stain resistance. Such innovations could find applications in various areas, including floor materials, waterproofing solutions, coatings, primers, wall coating, injection, sealing, castings, laminates, adhesives, and lining materials.

Applying biomimicry in civil engineering allows researchers to draw inspiration from hornets. Experts can demonstrate innovative approaches for promoting sustainable and efficient construction practices by imitating their process of converting plant materials into construction materials. Integrating biomimicry P-LM into wood construction enables achieving durable, eco-friendly solutions while promoting sustainable practices. Repairing wood with biomimicry P-LM combines the structural integrity of wood with the versatility of paper-based composites. Biomimicry P-LM infused with adhesive resins can reinforce and repair wood composite panels, extending their service life. Transforming biomimicry P-LM into fillers or adhesives enables the restoration of the integrity of wooden structures. Using biomimicry P-LM as paper-based coatings enhances wood's resistance to environmental factors. These coatings prevent decay, warping, or degradation of the wood over time. Biomimicry P-LM as paper-based materials offers aesthetic possibilities, making them ideal for decorative finishes on wood surfaces. These finishes can mimic natural wood grain, stone textures, or custom designs, providing endless possibilities for architectural expression and interior design.

Utilising biomimicry outer envelope P-LM in civil engineering through 3D printing opens up a range of possibilities for innovative

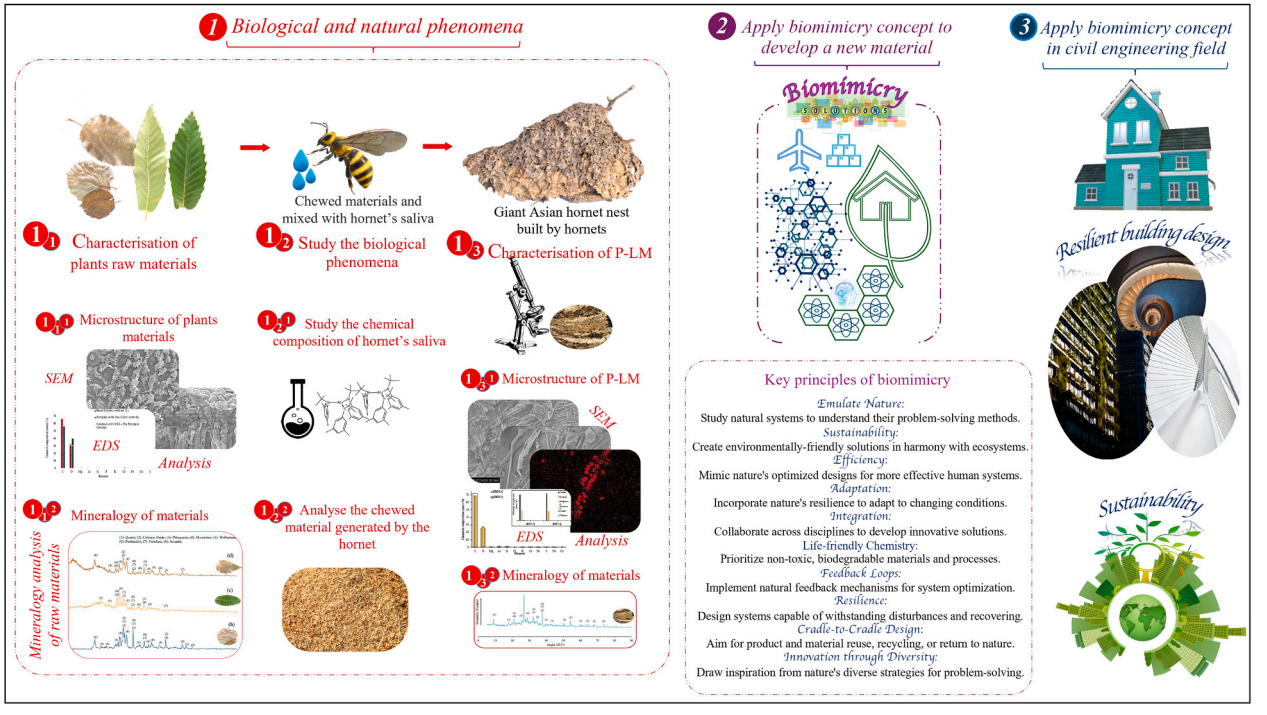

Fig. 18. Steps to biomimicry the paper-like materials generated by the Asian hornet to build their giant structure nest.

and sustainable construction practices. Structural components benefit from the strength of paper-based materials when appropriately reinforced, offering a lightweight alternative to traditional materials for panels. In disaster-stricken areas or regions facing housing shortages, the rapid construction of temporary shelters is crucial. This approach is particularly beneficial for temporary structures, lightweight buildings, or projects in remote areas where transporting heavy construction materials is challenging. Additionally, 3D printing with biomimicry P-LM provides a cost-effective and sustainable solution with minimal environmental impact due to the biodegradability of paper-based materials. Furthermore, infrastructure repair and maintenance can be facilitated by paper-based composites through 3D printing, effectively repairing and reinforcing existing structures while minimising environmental impact. By incorporating renewable and biodegradable paper-based materials, green building practices are enhanced, aligning construction processes with sustainability principles. Architectural innovation is also enabled, allowing for intricate designs and creativity in construction through 3D printing with paper-based materials, thus realising complex structures with precision and efficiency.

7. Limitations and challenges

This study represents a preliminary investigation into the microstructure, chemical composition, and mineralogy of the Asian hornet nest paper-like material (AHN P-LM) and surrounding tree leaves. While it provides an essential foundation, several technical, environmental, and economic challenges require further exploration to advance its application in material science and civil engineering fields. The integration of these materials into complex construction projects will require additional research, including structural analysis, mechanical performance studies, and modelling. The limitations and challenges associated with the biomimicry of the Asian hornet nest paper-like material are as follows:

- Synthetic replication of Asian hornet saliva: One notable challenge is replicating the intricate composition of hornet saliva, which serves as a crucial adhesive (binder) in the AHNs. Identifying a natural or synthetic alternative to this adhesive is essential for the feasibility of mass-producing of inspired AHN P-LM.
- Scaling up for large-scale construction: A significant challenge not addressed in this study is the scalability of AHN P-LM for use in large-scale construction projects, such as bridges or high-rise buildings. Our current focus is on material characterisation at the microstructural level, but the challenges of mass production and scaling need further exploration.
- Mechanical performance testing: Although this study examined the chemical composition and microstructure of the material, it lacks comprehensive mechanical testing (e.g., tensile strength, elasticity, and durability) to evaluate its performance under real-world conditions. Understanding how the material behaves under load and environmental stresses is crucial for its practical application.
- Manufacturing and industrial processes: This preliminarily study does not provide specific guidelines for efficiently manufacturing of the inspired AHN P-LM using current industrial technologies, such as 3D printing or mass production. Progressing this biomimetic material from the laboratory to practical construction applications will require a detailed exploration of its compatibility with existing manufacturing processes.
- Environmental impact: Another limitation of the study is the absence of a life cycle assessment (LCA) to evaluate the environmental impact of replicating and utilising AHN P-LM on a large scale. While our preliminary study suggests that using forest biomass as a raw material could give ecological benefits, a more comprehensive analysis is needed to assess the environmental consequences of sourcing, manufacturing, and deploying these types of materials.
- Biomimicry and regulatory standards: using biological models in civil engineering presents challenges related to regulatory standards and long-term performance. Biomimicry in civil engineering requires knowledge of both biological and engineering principles.
- Economic Feasibility: The potential cost of replicating and using inspired AHN P-LM compared to conventional construction materials remains unexplored. An economic study, which will include the cost-effectiveness of using forest biomass and low-tech manufacturing processes, is critical to assess the practical relevance of this material.

8. Conclusions

The results of this study are based on the microstructure, chemical composition, and mineralogy analyses of both tree leaves and the paper-like material (P-LM) that constitute the various components of the AHN (outer envelope and combs). The outer envelope P-LM mainly comprises plant-based materials such as softwood, hardwood, tree leaves, and grass components. Differences were observed in the microstructure of the outer envelope P-LM compared to the comb P-LM, both in shape and tissue composition. Nitrogen (N) was found in the EDS analysis of Asian hornet nest (AHN) P-LM, but it was absent in the analysed leaves. This finding implies that the nitrogen originates from the hornet's saliva, indicating a distinct contribution from the hornet's secretions to the composition of the nest material. The SEM-EDS analysis provides a critical understanding of the morphology and composition of calcium-containing grains within the outer envelope of the AHN's P-LM. This analysis further validates the XRD findings, confirming the presence of CaOx as a crystalline phase in the microstructure of the outer envelope. These findings hold significant implications for comprehending the formation and characteristics of the AHN and opening avenues for developing innovative biomimicry construction materials based on the chemical and structural attributes of these nests. The detection of inorganic minerals in the chemical composition analysis and mineralogy characterisation of the P-LM from Asian hornet nests could be attributed to three distinct possibilities. Firstly, these minerals may originate from the chemical composition of plant fragments, including leaves, grass, and softwood and hardwood. Secondly, environmental contamination may contribute to the minerals infiltrating the nest material through dust and the surrounding

environment, leading to a variation in mineral content. Lastly, it is important to emphasise the intriguing concept of the intentional incorporation of inorganic materials by Asian hornets during their nest-building process. Studying the AHNs can unlock a world of sustainable civil engineering solutions. Understanding these incredible creatures' behaviour and material composition can inspire the creation of eco-friendly construction materials and inventive building methods that can pave the way for effective and durable infrastructure developments.

CRediT authorship contribution statement

Sandra Pereira: Writing – review & editing, Validation, Supervision, Resources, Project administration, Investigation, Funding acquisition, Data curation, Conceptualization. **Miguel C. S. Nepomuceno:** Writing – review & editing, Validation, Investigation. **Ana P. Gomes:** Writing – review & editing, Validation, Investigation, Data curation. **Jorge Pinto:** Writing – review & editing, Validation, Supervision, Resources, Project administration, Funding acquisition, Conceptualization. **Naim Sedira:** Writing – review & editing, Writing – original draft, Visualization, Validation, Software, Methodology, Investigation, Formal analysis, Data curation, Conceptualization.

Declaration of Competing Interest

The authors declare that they have no known competing financial interests or personal relationships that could have appeared to influence the work reported in this paper.

Acknowledgements

This work was partially supported by the FCT (Portuguese Foundation for Science and Technology) through the project UIDB/04082/2020 (CMADE).

Data Availability

No data was used for the research described in the article.

References

[1] H.R. Mattila, G.W. Otis, J. Billen, L.T.P. Nguyen, S. Shimano, Comparison of the external morphology of the sternal glands for hornets in the Genus Vespa, Biology 11 (2) (2022), https://doi.org/10.3390/biology11020245.
[2] C. Herrera, A. Marqués, V. Colomar, M.M. LezaAnalysis of the Secondary Nest of the Yellow-legged Hornet Found in the Balearic Islands Reveals Its High Adaptability to Mediterranean Isolated Ecosystems, Isl. Invasives Scaling up to Meet Challenge. Proc. Int. Conf. Isl. Invasives 2017, no. 622019, 37538010.2305/iucn.ch.2019.ssc-op.62.en.
[3] J. Van Der Vecht, The Vespinae of the Indo-Malayan and Papuan Areas (Hymenoptera, Vespidae), Zool. Verh. 34 (1) (1957) 1–82. ⟨http://www.repository.naturalis.nl/record/317560%5Cnhttp://www.repository.naturalis.nl/document/148846⟩ ([Online]. Available).
[4] J. Van Der Vecht, Notes on oriental Vespinae, including some species from China and Japan (Hymenoptera, Vespidae),", Zool. Meded. 36 (13) (1959) 205–232. ⟨http://www.repository.naturalis.nl/record/318251⟩ ([Online]. Available).
[5] C. Ries, N. Schneider, F. Vitali, A. Weigand, First records and distribution of the invasive alien hornet *Vespa velutina nigrithorax* du Buysson, 1905 (Hymenoptera: Vespidae) in Luxembourg, Bull. la Soci. été Des. Nat. Luxemb. 123 (2021) 181–193.
[6] P.J. Kennedy, S.M. Ford, J. Poidatz, D. Thiéry, J.L. Osborne, Searching for nests of the invasive Asian hornet (Vespa velutina) using radio-telemetry, Commun. Biol. 1 (1) (2018), https://doi.org/10.1038/s42003-018-0092-9.
[7] J. Haxaire, J.-P. Tamisier, J.-P. Bouguet, Vespa velutina Lepeletier, 1836, une redoutable nouveauté pour la faune de France (Hym., Vespidae), Bull. De. la Soci. été Èntomol. De. Fr. 111 (2) (2006) 194, https://doi.org/10.3406/bsef.2006.16309.
[8] M. Arca, et al., Reconstructing the invasion and the demographic history of the yellow-legged hornet, vespa velutina, in Europe, Biol. Invasions 17 (8) (2015) 2357–2371, https://doi.org/10.1007/s10530-015-0880-9.
[9] K. Monceau, D. Thiery, The Asian Yellow-legged advance of implacable Hornet: the a bee-killer, Br. Wildl. (March 2018) (2017).
[10] G.E. Budge, et al., The invasion, provenance and diversity of Vespa velutina Lepeletier (Hymenoptera: Vespidae) in Great Britain, PLoS One 12 (9) (2017) 1–12, https://doi.org/10.1371/journal.pone.0185172.
[11] M. Matsuura, S. Yamane, Biology of the Vespine Wasps 23, Springer-Verlag, Berlin, 1990.
[12] O. de la Hera, M.L. Alonso, R.M. Alonso, Behaviour of Vespa velutina nigrithorax (Hymenoptera: Vespidae) under controlled environmental conditions, Insects (2023).
[13] A. Diéguez-Antón, O. Escuredo, M.C. Seijo, M.S. Rodríguez-Flores, Embryo, relocation and secondary nests of the invasive species Vespa velutina in Galicia (NW Spain), Animals 12 (20) (2022), https://doi.org/10.3390/ani12202781.
[14] N. Sedira, J. Pinto, M. Ginja, A.P. Gomes, M.C.S. Nepomuceno, S. Pereira, Investigating the architecture and characteristics of asian hornet nests: a biomimetics examination of structure and materials, Materials (2023).
[15] X.F. Sánchez, R.J. Charles, Notes on the nest architecture and colony composition in winter of the yellow-legged asian hornet, vespa velutina lepeletier 1836 (Hym.: Vespidae), in its introduced habitat in galicia (NW Spain), Insects 10 (8) (2019), https://doi.org/10.3390/insects10080237.
[16] J.M. Benyus, Biomimicry: Innovation Inspired by Nature, HarperCollins Publishers Ltd, London, 1997.
[17] N. Verbrugghe, E. Rubinacci, A.Z. Khan, Biomimicry in architecture: a review of definitions, case studies, and design methods, Biomimetics 8 (1) (2023), https://doi.org/10.3390/biomimetics8010107.
[18] M.S. Aziz, A.Y. El Sherif, Biomimicry as an approach for bio-inspired structure with the aid of compu tation, Alex. Eng. J. 55 (1) (2016) 707–714, https://doi.org/10.1016/j.aej.2015.10.015.
[19] What Is Biomimicry? – Biomimicry Institute ⟨https://biomimicry.org/what-is-biomimicry/#⟩ (accessed Feb. 29, 2024).
[20] M. AlAli, Y. Mattar, M.A. Alzaim, S. Beheiry, Applications of biomimicry in architecture, construction and civil engineering, Biomimetics 8 (2) (2023), https://doi.org/10.3390/biomimetics8020202.
[21] Y.S. Kim, W.S. Na, Implementation of biomimicry for detecting composite structure damage using impedance-based non-destructive testing method, Appl. Sci. 13 (2) (2023), https://doi.org/10.3390/app13020876.

[22] Q. Li, Z. Liu, W. Chen, B. Yuan, X. Liu, W. Chen, A novel bio-inspired bone-mimic self-healing cement paste based on hydroxyapatite formation, Cem. Concr. Compos. 104 (June) (2019) 103357, https://doi.org/10.1016/j.cemconcomp.2019.103357.
[23] N. Hu, P. Feng, G. Dai, The gift from nature: Bio-inspired strategy for developing innovative bridges, J. Bionic Eng. 10 (4) (2013) 405–414, https://doi.org/10.1016/S1672-6529(13)60246-2.
[24] S. Hayes, C. Desha, D. Baumeister, Learning from nature – Biomimicry innovation to support infrastructure sustainability and resilience, Technol. Forecast. Soc. Change 161 (September) (2020) 120287, https://doi.org/10.1016/j.techfore.2020.120287.
[25] N. Imani, B. Vale, A framework for finding inspiration in nature: biomimetic energy efficient building design, Energy Build. 225 (2020) 110296, https://doi.org/10.1016/j.enbuild.2020.110296.
[26] D.G. Soltan, V.C. Li, Nacre-inspired composite design approaches for large-scale cementitious members and structures, Cem. Concr. Compos. 88 (2018) 172–186, https://doi.org/10.1016/j.cemconcomp.2018.02.006.
[27] P. Gunasekaran, S.N.S. Subramanian, A. Sekar, Optimizing mesh sizes of thin shells using biomimicry for a sustainable solution, J. Biomim. Biomater. Biomed. Eng. 61 (2023) 1–14, https://doi.org/10.4028/P-XYCL3M.
[28] M. Vishali, A. Bahrami, K.S. Satyanarayanan, V. Thirumurugan, M. Prakash, Effects of using different materials at interface of trapezoidal reinforced concrete infilled frames–analytical and experimental approaches, Front. Mater. 10 (December) (2023) 1–19, https://doi.org/10.3389/fmats.2023.1239312.
[29] R. Sanga, M. Kilumile, F. Mohamed, Alternative clay bricks inspired from termite mound biomimicry, Case Stud. Constr. Mater. 16 (February) (2022), https://doi.org/10.1016/j.cscm.2022.e00977.
[30] N. Sedira, J. Pento, I. Bentes, S. Pereira, Bibliometric analysis of global research trends on biomimetics, biomimicry, bionics, and bio-inspired concepts in civil engineering using the Scopus database, Bioinspir. Biomim. 041001 (19) (2024) 56, https://doi.org/10.1088/1748-3190/ad3ff6.
[31] N. Sedira, J. Castro-Gomes, Alkali-activated binders based on tungsten mining waste and electric-arc-furnace slag: compressive strength and microstructure properties, CivilEng 1 (2) (2020) 154–180, https://doi.org/10.3390/civileng1020010.
[32] K.J. Lendzian, Survival strategies of plants during secondary growth: barrier properties of phellems and lenticels towards water, oxygen, and carbon dioxide, J. Exp. Bot. 57 (11) (2006) 2535–2546, https://doi.org/10.1093/jxb/erl014.
[33] J.S. Boyer, Turgor and the transport of CO2 and water across the cuticle (epidermis) of leaves, J. Exp. Bot. 66 (9) (2015) 2625–2633, https://doi.org/10.1093/jxb/erv065.
[34] X. Wang, C. Shen, P. Meng, G. Tan, L. Lv, Analysis and review of trichomes in plants, BMC Plant Biol. 21 (1) (2021) 1–11, https://doi.org/10.1186/s12870-021-02840-x.
[35] J. Negi, M. Hashimoto-Sugimoto, K. Kusumi, K. Iba, New approaches to the biology of stomatal guard cells, Plant Cell Physiol. 55 (2) (2014) 241–250, https://doi.org/10.1093/pcp/pct145.
[36] S. Margaret Fank-de-carvalho, M. ROdrigues De Aguiar Gomes, P. 蚊ALO Tanno Silva, S. NAIR B置, Leaf surfaces of Gomphrena spp. (Amaranthaceae) from Cerrado biome, Biocell 34 (1) (2010) 23–36, https://doi.org/10.32604/biocell.2010.34.023.
[37] J.J. Xi, et al., Sodium-related adaptations to drought: new insights from the xerophyte plant zygophyllum xanthoxylum, Front. Plant Sci. 871 (ember) (2018) 1–15, https://doi.org/10.3389/fpls.2018.01678.
[38] G.A. Gambetta, J.C. Herrera, S. Dayer, Q. Feng, U. Hochberg, S.D. Castellarin, The physiology of drought stress in grapevine: towards an integrative definition of drought tolerance, J. Exp. Bot. 71 (16) (2020) 4658–4676, https://doi.org/10.1093/jxb/eraa245.
[39] Y. Lu, Y. Hu, R.L. Snyder, E.R. Kent, Tea leaf's microstructure and ultrastructure response to low temperature in indicating critical damage temperature, Inf. Process. Agric. 6 (2) (2019) 247–254, https://doi.org/10.1016/j.inpa.2018.09.004.
[40] M. Chen, The tea plant leaf cuticle: from plant protection to tea quality, Front. Plant Sci. 12 (October) (2021) 1–13, https://doi.org/10.3389/fpls.2021.751547.
[41] S. Matschi, et al., Structure-function analysis of the maize bulliform cell cuticle and its potential role in dehydration and leaf rolling, Plant Direct 4 (10) (2020) 1–21, https://doi.org/10.1002/pld3.282.
[42] M. Riederer, L. Schreiber, Protecting against water loss: analysis of the barrier properties of plant cuticles, J. Exp. Bot. 52 (363) (2001) 2023–2032, https://doi.org/10.1093/jexbot/52.363.2023.
[43] D. Di Baccio, A. Minnocci, L. Sebastiani, Leaf structural modifications in Populus × euramericana subjected to Zn excess, Biol. Plant. 54 (3) (2010) 502–508, https://doi.org/10.1007/s10535-010-0088-x.
[44] L.A. Ivanova, V.I. P'yankov, Structural adaptation of the leaf mesophyll to shading, Russ. J. Plant Physiol. 49 (3) (2002) 419–431, https://doi.org/10.1023/A:1015513607202.
[45] E.M. Yahia, A. Carrillo-López, G.M. Barrera, H. Suzán-Azpiri, M.Q. Bolaños, Photosynthesis, Elsevier Inc., 2018.
[46] W.H. Outlaw, C.L. Schmuck, N.E. Tolbert, Photosynthetic carbon metabolism in the palisade parenchyma and Spongy Parenchyma of Vicia faba L, Plant Physiol. 58 (2) (1976) 186–189, https://doi.org/10.1104/pp.58.2.186.
[47] A.L. Baillie, A.J. Fleming, The developmental relationship between stomata and mesophyll airspace, N. Phytol. 225 (3) (2020) 1120–1126, https://doi.org/10.1111/nph.16341.
[48] K.J. Niklas, The Evolutionary Biology of Plants, University of Chicago Press, Chicago, 1997.
[49] C.M. Pueschel, Calcium oxalate mineralisation in the algae, Phycologia 58 (4) (2019) 331–350, https://doi.org/10.1080/00318884.2019.1578587.
[50] M.A. Webb, Cell-mediated crystallization of calcium oxalate in plants, Plant Cell 11 (4) (1999) 751–761, https://doi.org/10.1105/tpc.11.4.751.
[51] R. Prasad, Y.S. Shivay, Oxalic acid/oxalates in plants: from self-defence to phytoremediation, Curr. Sci. 112 (8) (2017) 1665–1667, https://doi.org/10.18520/cs/v112/i08/1665-1667.
[52] M. Chwil, M. Kostryco, Histochemical assays of secretory trichomes and the structure and content of mineral nutrients in Rubus idaeus L. leaves, Protoplasma 257 (1) (2020) 119–139, https://doi.org/10.1007/s00709-019-01426-7.
[53] W. R. J. Van Cotthem, A classification of stomatal types, Bot. J. Linn. Soc. 63 (3) (1970) 235–246, https://doi.org/10.1111/j.1095-8339.1970.tb02321.x.
[54] E.L. Harrison, L. Arce Cubas, J.E. Gray, C. Hepworth, The influence of stomatal morphology and distribution on photosynthetic gas exchange, Plant J. 101 (4) (2020) 768–779, https://doi.org/10.1111/tpj.14560.
[55] P.J. Franks, G.D. Farquhar, The mechanical diversity of stomata and its significance in gas-exchange control, Plant Physiol. 143 (1) (2007) 78–87, https://doi.org/10.1104/pp.106.089367.
[56] P.J. White, Long-distance Transport in the Xylem and Phloem, Elsevier Ltd., 2011.
[57] S. Torre, Morphology and Anatomy | Leaves. Encyclopedia of Rose Science, Elsevier, 2003, pp. 497–504, https://doi.org/10.1016/B0-12-227620-5/00119-1.
[58] K. Růžička, R. Ursache, J. Hejátko, Y. Helariutta, Xylem development - from the cradle to the grave, N. Phytol. 207 (3) (2015) 519–535, https://doi.org/10.1111/nph.13383.
[59] B.G. Hwang, J. Ryu, S.J. Lee, Vulnerability of protoxylem and metaxylem vessels to embolisms and radial refilling in a vascular bundle of maize leaves, Front. Plant Sci. 7 (June) (2016) 1–10, https://doi.org/10.3389/fpls.2016.00941.
[60] A. Emonet, A. Hay, Development and diversity of lignin patterns, Plant Physiol. 190 (1) (2022) 31–43, https://doi.org/10.1093/plphys/kiac261.
[61] H. Kim, J.Y. Lee, A method for a rapid and accurate detection of phloem sieve element development: its application and scalability, J. Plant Biol. 65 (1) (2022) 1–10, https://doi.org/10.1007/s12374-021-09334-1.
[62] P. Kaur, P. Gonzalez, M. Dutt, E. Etxeberria, Identification of sieve elements and companion cell protoplasts by a combination of brightfield and fluorescence microscopy, Appl. Plant Sci. 6 (9) (2018) 1–8, https://doi.org/10.1002/aps3.1179.
[63] D.M. Braun, L. Wang, Y.L. Ruan, Understanding and manipulating sucrose phloem loading, unloading, metabolism, and signalling to enhance crop yield and food security, J. Exp. Bot. 65 (7) (2014) 1713–1735, https://doi.org/10.1093/jxb/ert416.
[64] T.J. McCubbin, D.M. Braun, Phloem anatomy and function as shaped by the cell wall, J. Plant Physiol. 266 (June) (2021) 153526, https://doi.org/10.1016/j.jplph.2021.153526.

[65] C.D. Jiang, X. Wang, H.Y. Gao, L. Shi, W.S. Chow, Systemic regulation of leaf anatomical structure, photosynthetic performance, and high-light tolerance in sorghum, Plant Physiol. 155 (3) (2011) 1416–1424, https://doi.org/10.1104/pp.111.172213.
[66] N. Mehle, et al., Phytoplasmas associated with declining of hazelnut (Corylus avellana) in Slovenia, Eur. J. Plant Pathol. 155 (4) (2019) 1117–1132, https://doi.org/10.1007/s10658-019-01839-3.
[67] G. Karabourniotis, G. Liakopoulos, D. Nikolopoulos, P. Bresta, Protective and defensive roles of non-glandular trichomes against multiple stresses: structure–function coordination, J. For. Res. 31 (1) (2020) 1–12, https://doi.org/10.1007/s11676-019-01034-4.
[68] R. Romero-Aranda, R. Cantó-Garay, P.F. Martínez, Distribution and density of stomata in two cultivars of Gerbera jamesonii and its relation to leaf conductance, Sci. Hortic. 58 (1–2) (1994) 167–173, https://doi.org/10.1016/0304-4238(94)90137-6.
[69] V.J. Anderson, D.D. Briske, Stomatal distribution, density and conductance of three perennial grasses native to the Southern true Prairie of Texas, Am. Midl. Nat. 123 (1) (1990) 152–159.
[70] C. Kuan, S.L. Yang, C.M.K. Ho, Using quantitative methods to understand leaf epidermal development, Quant. Plant Biol. 3 (2022), https://doi.org/10.1017/qpb.2022.25.
[71] C.D. Whitewoods, Riddled with holes: Understanding air space formation in plant leaves, PLoS Biol. 19 (12) (2021) e3001475, https://doi.org/10.1371/journal.pbio.3001475.
[72] V.R. Franceschi, P.A. Nakata, Calcium oxalate in plants: formation and function, Annu. Rev. Plant Biol. 56 (2005) 41–71, https://doi.org/10.1146/annurev.arplant.56.032604.144106.
[73] U.M. dos Santos, J.F. de Carvalho Gonçalves, T.R. Feldpausch, Growth, leaf nutrient concentration and photosynthetic nutrient use efficiency in tropical tree species planted in degraded areas in central Amazonia, For. Ecol. Manag. 226 (1–3) (2006) 299–309, https://doi.org/10.1016/j.foreco.2006.01.042.
[74] R.T.W. Siegwolf, J.R. Brooks, J. Roden, M. Saurer, Stable Isotopes in Tree Rings: Inferring Physiological, Climatic and Environmental Responses, Springer International Publishing, 2022.
[75] M. Tränkner, E. Tavakol, B. Jákli, Functioning of potassium and magnesium in photosynthesis, photosynthate translocation and photoprotection, Physiol. Plant. 163 (3) (2018) 414–431, https://doi.org/10.1111/ppl.12747.
[76] N. Ahmed, et al., The power of magnesium: unlocking the potential for increased yield, quality, and stress tolerance of horticultural crops, Front. Plant Sci. 14 (October) (2023) 1–25, https://doi.org/10.3389/fpls.2023.1285512.
[77] D. at the C. of S. C. S, A. C. P. in Sanders, J. Pelloux, C. Brownlee, J.F. Harper, Calcium at the Crossroads of Signaling. Plant Cell, 2002, pp. 401–417, 1410.1105/tpc.002899.
[78] M.D. Bootman, G. Bultynck, Fundamentals of cellular calcium signaling: a primer, Cold Spring Harb. Perspect. Biol. 12 (1) (2020) 1–16, https://doi.org/10.1101/cshperspect.a038802.
[79] K. Ravet, M. Pilon, Copper and iron homeostasis in plants: the challenges of oxidative stress, Antioxid. Redox Signal 19 (9) (2013) 919–932, https://doi.org/10.1089/ars.2012.5084.
[80] Y.S. Fernandes, L.M.P. Trindade, M.H. Rezende, J.R. Paula, L.A. Gonçalves, Trichomes and chemical composition of the volatile oil of Trichogonia cinerea (Gardner) R. M. King & H. Rob. (Eupatorieae, Asteraceae), An. Acad. Bras. Cienc. 88 (1) (2016) 309–322, https://doi.org/10.1590/0001-3765201520140660.
[81] D.J. Wang, J.W. Zeng, W.T. Ma, M. Lu, H.M. An, Morphological and structural characters of trichomes on various organs of Rosa roxburghii, HortScience 54 (1) (2019) 45–51, https://doi.org/10.21273/HORTSCI13485-18.
[82] J. Ďurkovič, et al., The effects of propagation techniques on leaf vascular anatomy, modulus of elasticity, and photosynthetic traits in micropropagated and grafted plants of the dutch elm hybrid 'Dodoens, J. Am. Soc. Hortic. Sci. 141 (4) (2016) 351–362, https://doi.org/10.21273/jashs.141.4.351.
[83] S.M. Ickert-Bond, A.J. Harris, S. Lutz, J. Wen, A detailed study of leaf micromorphology and anatomy of New World Vitis L. subgenus Vitis within a phylogenetic and ecological framework reveals evolutionary convergence, J. Syst. Evol. 56 (4) (2018) 309–330, https://doi.org/10.1111/jse.12313.
[84] C. Naidoo, Y. Naidoo, Y.H. Dewir, The secretory apparatus of Tabernaemontana ventricosa Hochst. ex A.DC. (Apocynaceae): Laticifer identification, characterization and distribution Clarissa, Plants 9 (686) (2020).
[85] J. Zhang, H. Lu, L. Huang, Calciphytoliths (calcium oxalate crystals) analysis for the identification of decayed tea plants (Camellia sinensis L.), Sci. Rep. 4 (2014) 1–9, https://doi.org/10.1038/srep06703.
[86] T.S.M.A. El-Alfy, H.M.A. El-Gohary, N.M. Sokkar, S.A. El-Tawab, D.A.M. Al-Mahdy, Botanical and genetic characteristics of Celtis australis L. and Celtis occidentalis L. grown in Egypt, Bull. Fac. Pharm. Cairo Univ. 49 (1) (2011) 37–57, https://doi.org/10.1016/j.bfopcu.2011.07.007.
[87] V. Franceschi, Calcium oxalate in plants, Trends Plant Sci. 6 (7) (2001) 331, https://doi.org/10.1016/s1360-1385(01)02014-3.
[88] M. Malekhosseini, et al., Traces of calcium oxalate biomineralization in fossil leaves from late Oligocene maar deposits from Germany, Sci. Rep. 12 (1) (2022) 1–15, https://doi.org/10.1038/s41598-022-20144-4.
[89] I.T. Cerritos-Castro, et al., Amaranth calcium oxalate crystals are associated with chloroplast structures and proteins, Microsc. Res. Tech. 85 (11) (2022) 3694–3706, https://doi.org/10.1002/jemt.24221.
[90] H.J. Ensikat, M. Malekhosseini, J. Rust, M. Weigend, Visualisation of calcium oxalate crystal macropatterns in plant leaves using an improved fast preparation method, J. Microsc. 290 (3) (2023) 168–177, https://doi.org/10.1111/jmi.13187.
[91] R.F. Parsons, P.M. Attiwill, N.C. Uren, P.M. Kopittke, Calcium oxalate and calcium cycling in forest ecosystems, Trees Struct. Funct. 36 (2) (2022) 531–536, https://doi.org/10.1007/s00468-021-02226-4.
[92] K. Kudô, et al., Nest materials and some chemical characteristics of nests of a new world swarm-founding polistine wasp, Polybia paulista (Hymenoptera Vespidae), Ethol. Ecol. Evol. 13 (4) (2001) 351–360, https://doi.org/10.1080/08927014.2001.9522766.
[93] R. Klingner, K. Richter, E. Schmolz, B. Keller, The role of moisture in the nest thermoregulation of social wasps, Naturwissenschaften 92 (9) (2005) 427–430, https://doi.org/10.1007/s00114-005-0012-y.
[94] J.G. Haase, L.H. Leung, P.D. Evans, Plasma pre-treatments to improve theweather resistance of polyurethane coatings on black spruce wood, Coatings 9 (1) (2019), https://doi.org/10.3390/coatings9010008.
[95] B. Choat, A.R. Cobb, S. Jansen, Structure and function of bordered pits: new discoveries and impacts on whole-plant hydraulic function, N. Phytol. 177 (3) (2008) 608–626, https://doi.org/10.1111/j.1469-8137.2007.02317.x.
[96] Y. Sano, Bordered pit structure and cavitation resistance in woody plants, Second. Xylem Biol. Orig. Funct. Appl. (Jan. 2016) 113–130, https://doi.org/10.1016/B978-0-12-802185-9.00007-3.
[97] M.M. Khandaker, et al., Enhancing Rubisco gene expression and metabolites accumulation for better plant growth in Ficus deltoidea under drought stress using hydrogen peroxide, Front. Plant Sci. 13 (2022), https://doi.org/10.3389/fpls.2022.965765.
[98] K. Billakurthi, J.M. Hibberd, A rapid and robust leaf ablation method to visualize bundle sheath cells and chloroplasts in C3 and C4 grasses, Plant Methods 19 (1) (2023) 1–11, https://doi.org/10.1186/s13007-023-01041-x.
[99] E. Maai, H. Miyake, M. Taniguchi, Differential positioning of chloroplasts in C4 mesophyll and bundle sheath cells, Plant Signal. Behav. 6 (8) (2011) 1111–1113, https://doi.org/10.4161/psb.6.8.15809.
[100] L. Hua, S.R. Stevenson, I. Reyna-Llorens, H. Xiong, S. Kopriva, J.M. Hibberd, The bundle sheath of rice is conditioned to play an active role in water transport as well as sulfur assimilation and jasmonic acid synthesis, Plant J. 107 (1) (2021) 268–286, https://doi.org/10.1111/tpj.15292.
[101] R. Roth, L.N. Hall, T.P. Brutnell, J.A. Langdale, Bundle sheath defective2, a mutation that disrupts the coordinated development of bundle sheath and mesophyll cells in the maize leaf, Plant Cell 8 (5) (1996) 915–927, https://doi.org/10.2307/3870292.
[102] C.L.D. Jenkins, S. Boag, Isolation of bundle sheath cell chloroplasts from the NADP-ME Type C4 Plant zea mays capacities for CO2 assimilation and malate decarboxylation, Plant Physiol. 79 (1985) 84–89.
[103] K. Andersen, J. Bain, D. Bishop, R. Smillie, Photosystem II activity in agranal bundle sheath chloroplasts from zea mays, Plant Physiol. 49 (4) (1972) 461–466, https://doi.org/10.1104/pp.49.4.461.
[104] W. Majeran, Y. Cai, Q. Sun, K.J. Van Wijk, Functional differentiation of bundle sheath and mesophyll maize chloroplasts determined by comparative proteomics, Plant Cell 17 (11) (2005) 3111–3140, https://doi.org/10.1105/tpc.105.035519.

[105] G.E. Edwards, C.C. Black, Isolation of mesophyll cells and bundle sheath cells from Digitaria sanguinalis (L.) Scop. Leaves and a scanning microscopy study of the internal leaf cell morphology, Plant Physiol. 47 (1) (1971) 149–156, https://doi.org/10.1104/pp.47.1.149.
[106] R. Shmulsky, P.D. Jones, Forest Products and Wood Science: An Introduction, 7th ed., Wiley-Blackwell, 2019.
[107] Di Tamburini, C.R. Cartwright, G. Cofta, M. Zborowska, M. Mamoňová, Distinguishing the signs of fungal and burial-induced degradation in waterlogged wood from Biskupin (Poland) by scanning electron microscopy, Microsc. Microanal. 24 (2) (2018) 163–182, https://doi.org/10.1017/S143192761800020X.
[108] W. Ruayruay, S. Khongtong, Impregnation of natural rubber into rubber wood: a green wood composite, BioResources 9 (3) (2014) 5438–5447, https://doi.org/10.15376/biores.9.3.5438-5447.
[109] Y. Huang, Y. Han, L. Wei, J. Wang, Comparative studies of tracheary element structure of some gymnosperms with angiosperms, Am. J. Plant Sci. 08 (05) (2017) 959–984, https://doi.org/10.4236/ajps.2017.85064.
[110] I.C. Osterkamp, et al., Changes of wood anatomical characters of selected species of araucaria during artificial charring: implications for palaeontology, Acta Bot. Bras. 32 (2) (2018) 198–211, https://doi.org/10.1590/0102-33062017abb0360.
[111] D. Keunecke, S. Hering, P. Niemz, Three-dimensional elastic behaviour of common yew and Norway spruce, Wood Sci. Technol. 42 (8) (2008) 633–647, https://doi.org/10.1007/s00226-008-0192-7.
[112] D. Chen, L.D. Melton, D.J. McGillivray, T.M. Ryan, P.J. Harris, Changes in the orientations of cellulose microfibrils during the development of collenchyma cell walls of celery (Apium graveolens L.), Planta 250 (6) (2019) 1819–1832, https://doi.org/10.1007/s00425-019-03262-8.
[113] X.L. Jia, et al., De novo assembly, transcriptome characterization, lignin accumulation, and anatomic characteristics: novel insights into lignin biosynthesis during celery leaf development, Sci. Rep. 5 (2015) 1–14, https://doi.org/10.1038/srep08259.
[114] C.E.J. Botha, R.H.M. Cross, J. Gerber, The microstructure of plasmodesmata in internodal stem tissue of the Saccharum hybrid var. NCo376: evidence for an apoplasmic loading pathway, S. Afr. J. Sci. 100 (11–12) (2004) 619–623.
[115] P. Kitin, T. Fujii, H. Abe, K. Takata, Anatomical features that facilitate radial flow across growth rings and from xylem to cambium in Cryptomeria japonica, Ann. Bot. 103 (7) (2009) 1145–1157, https://doi.org/10.1093/aob/mcp050.
[116] S. Higuchi, D. Aoki, Y. Matsushita, M. Yoshida, S. Yagami, K. Fukushima, The 'chi-chi' of Ginkgo biloba L. grows downward with horizontally curving tracheids having compression-wood-like features, J. Wood Sci. 69 (1) (2023), https://doi.org/10.1186/s10086-023-02102-4.
[117] Y. Liu, Y. Huang, Q. Huang, F. Li, X. Liu, Liquid-phase deposition functionalized wood sponges for oil/water separation, J. Mater. Sci. 56 (34) (2021) 19075–19092, https://doi.org/10.1007/s10853-021-06440-w.
[118] A. van der Ent, et al., X-ray fluorescence elemental mapping of roots, stems and leaves of the nickel hyperaccumulators Rinorea cf. bengalensis and Rinorea cf. javanica (Violaceae) from Sabah (Malaysia), Borneo, Plant Soil 448 (1–2) (2020) 15–36, https://doi.org/10.1007/s11104-019-04386-2.
[119] A. Hedayati, H. Sefidari, C. Boman, N. Skoglund, N. Kienzl, M. Öhman, Ash transformation during single-pellet gasification of agricultural biomass with focus on potassium and phosphorus, Fuel Process. Technol. 217 (March) (2021), https://doi.org/10.1016/j.fuproc.2021.106805.
[120] F. Rees, et al., Metal immobilization on wood-derived biochars: distribution and reactivity of carbonate phases, J. Environ. Qual. 46 (4) (2017) 845–854, https://doi.org/10.2134/jeq2017.04.0152.
[121] N.R. Lersten, H.T. Horner, Development of the calcium oxalate crystal macropattern in pomegranate (Punica granatum, Punicaceae), Am. J. Bot. 92 (12) (2005) 1935–1941, https://doi.org/10.3732/ajb.92.12.1935.
[122] Kazuyoshi Endo, Toshihiro Kogure, Hiromichi Nagasawa, Biomineralization from molecular and nano-structural analyses to environmental science, 14th Int. Symp. Biominer. (2017) 393.
[123] R. Minocha, B. Chamberlain, S. Long, S.A. Turlapati, G. Quigley, Extraction and estimation of the quantity of calcium oxalate crystals in the foliage of conifer and hardwood trees, Tree Physiol. 35 (5) (2015) 574–580, https://doi.org/10.1093/treephys/tpv031.
[124] S.T. Konyar, N. Öztürk, F. Dane, Occurrence, types and distribution of calcium oxalate crystals in leaves and stems of some species of poisonous plants, Bot. Stud. 55 (1) (2014) 1–9, https://doi.org/10.1186/1999-3110-55-32.
[125] M. Haouzi, J. Gévar, A. Khalil, E. Darrouzet, Nest structures display specific hydrocarbon profiles: insights into the chemical ecology of the invasive yellow-legged hornet Vespa velutina nigrithorax, Chemoecology 31 (4) (2021) 227–238, https://doi.org/10.1007/s00049-021-00343-7.
[126] C. Larisch, et al., Poplar wood rays are involved in seasonal remodeling of tree physiology, Plant Physiol. 160 (3) (2012) 1515–1529, https://doi.org/10.1104/pp.112.202291.
[127] Y. Li, Q. Jin, D. Yang, J. Cui, Molybdenum sulfide induce growth enhancement Effect of rice (Oryza sativa L.) through regulating the synthesis of chlorophyll and the expression of aquaporin gene, J. Agric. Food Chem. 66 (16) (2018) 4013–4021, https://doi.org/10.1021/acs.jafc.7b05940.
[128] P.J. White, M.R. Broadley, Calcium in plants, Ann. Bot. 92 (4) (2003) 487–511, https://doi.org/10.1093/aob/mcg164.
[129] D.T. Clarkson, Calcium transport between tissues and its distribution in the plant, Plant Cell Environ. 7 (6) (1984) 449–456, https://doi.org/10.1111/j.1365-3040.1984.tb01435.x.
[130] C.A.E. Strömberg, V.S. Di Stilio, Z. Song, Functions of phytoliths in vascular plants: an evolutionary perspective, Funct. Ecol. 30 (8) (2016) 1286–1297, https://doi.org/10.1111/1365-2435.12692.
[131] C.J. Prychid, P.J. Rudall, M. Gregory, Systematics and biology of silica bodies in monocotyledons 69 (April) (2004).
[132] E. Trembath-Reichert, J.P. Wilson, S.E. McGlynn, W.W. Fischer, Four hundred million years of silica biomineralization in land plants, Proc. Natl. Acad. Sci. U. S. A. 112 (17) (2015) 5449–5454, https://doi.org/10.1073/pnas.1500289112.
[133] B. Briefing, Silica in plants: biological, biochemical and chemical studies, Ann. Bot. (2007) 1383–1389, https://doi.org/10.1093/aob/mcm247.
[134] J.D. Ovington, H.A.I. Madgwick, The sodium, potassium and phosphorus contents of tree species grown in close stands, N. Phytol. 57 (3) (1958) 273–284, https://doi.org/10.1111/j.1469-8137.1958.tb05316.x.
[135] Y. Wang, Y.F. Chen, W.H. Wu, Potassium and phosphorus transport and signaling in plants, J. Integr. Plant Biol. 63 (1) (2021) 34–52, https://doi.org/10.1111/jipb.13053.
[136] L.D.B. Suriyagoda, et al., Phosphorus fractions in leaves, N. Phytol. 237 (4) (2023) 1122–1135, https://doi.org/10.1111/nph.18588.
[137] V. Kumar, A. Sharma, P. Bakshi, R. Bhardwaj, A.K. Thukral, Multivariate analysis on the distribution of elements in plants, Acta Physiol. Plant. 40 (11) (2018) 1–29, https://doi.org/10.1007/s11738-018-2765-x.
[138] M. Nieves-Cordones, F.R. Al Shiblawi, H. Sentenac, Roles and transport of sodium and potassium in plants, Met. Ions Life Sci. 16 (2016) 291–324, https://doi.org/10.1007/978-3-319-21756-7_9.
[139] Y. Zhai, L. Cui, X. Zhou, Y. Gao, T. Fei, W. Gao, Estimation of nitrogen, phosphorus, and potassium contents in the leaves of different plants using laboratory-based visible and near-infrared reflectance spectroscopy: Comparison of partial least-square regression and support vector machine regression met,", Int. J. Remote Sens. 34 (7) (2013) 2502–2518, https://doi.org/10.1080/01431161.2012.746484.
[140] I. Carevic, N. Štirmer, M. Serdar, N. Ukrainczyk, Effect of wood biomass ash storage on the properties of cement composites, Materials 14 (7) (2021), https://doi.org/10.3390/ma14071632.
[141] E.A.-M.E. Kenneth W.B. Richard A. B, B. G.N, J.W. Anthony, R.A. Bideaux, K.W. Bladh, and M.C. Nichols, Handbook of Mineralogy. Chantilly: VA 20151-1110, USA, 2010.
[142] X. Yao, K. Xu, Y. Liang, Comparative analysis of the physical and chemical properties of different biomass ashes produced from various combustion conditions, BioResources 12 (2) (2017) 3222–3225, https://doi.org/10.15376/BIORES.12.2.3222-3235.
[143] D. Mardina, D. Asmi, M. Badaruddin, A.Z. Syahrial, Preparation of synthetic β-wollastonite produced from amorphous sio2 bamboo leaf ash and meretix shell, Mater. Sci. Forum 1029 (2021) 167–173, https://doi.org/10.4028/www.scientific.net/MSF.1029.167.
[144] S. Liodakis, G. Katsigiannis, G. Kakali, Ash properties of some dominant Greek forest species, Thermochim. Acta 437 (1–2) (2005) 158–167, https://doi.org/10.1016/j.tca.2005.06.041.
[145] IARC, ARC Working Group on the Evaluation of Carcinogenic Risks to Humans. Arsenic, Metals, Fibres and Dusts, Lyon (FR): International Agency for Research on Cancer; (IARC Monographs on the Evaluation of Carcinogenic Risks to Humans, No. 100C.) Silica Dust, Crystalline, in the Form of Quartz Or Cristobalite, 2012.

[146] I.J. Smalley, R. Kumar, K. O'Hara Dhand, I.F. Jefferson, R.D. Evans, The formation of silt material for terrestrial sediments: particularly loess and dust,, Sediment. Geol. 179 (3–4) (2005) 321–328, https://doi.org/10.1016/j.sedgeo.2005.06.011.
[147] IARC, "IARC Monographs on the Evaluation of Carcinogenic Risks to Humans: Silica, Some Silicates, Coal Dust and Para-aramid Fibrils," Lyon, France: World Health Organization, International Agency for Research on Cancer., 1997.
[148] NIOSH, Health effects of occupational exposure to respirable crystalline silica, NIOSH Hazard. Rev. (April) (2002) 145.
[149] J. Rabovsky, Biogenic amorphous silica: future research directions and areas of focus, Scand. J. Work Environ. Heal. 21 (2) (1995) 108–110.
[150] S.L. Holmberg, T. Claesson, Mineralogy of granulated wood ash from a heating plant in Kalmar, Sweden, Environ. Geol. 40 (7) (2001) 820–828, https://doi.org/10.1007/s002540100261.
[151] M. Hansell, Animal Architecture, Oxford University Press Inc., New York, 2005.
[152] J. Xie, et al., Bioprocess-inspired fabrication of materials with new structures and functions, Prog. Mater. Sci. 105 (March 2018) (2019) 100571, https://doi.org/10.1016/j.pmatsci.2019.05.004.
[153] J. Zhu, S. Chowdhury, Building resilience in civil infrastructure systems: system-level biomimicry to address complex managerial challenges, J. Infrastruct. Syst. 28 (1) (Dec. 2022) 06021002, https://doi.org/10.1061/(asce)is.1943-555x.0000665.
[154] M. Imani, M. Donn, Z. Balador, Bio-inspired materials: contribution of biology to energy efficiency of buildings, Handb. Ecomater. 3 (2019) 2213–2236, https://doi.org/10.1007/978-3-319-68255-6_136.
[155] W. Li, et al., Recent advances in intrinsic self-healing cementitious materials, Adv. Mater. 30 (17) (2018) 1–9, https://doi.org/10.1002/adma.201705679.